sustainability

MDPI

Article

Agro-Industrial Waste Upcycling into Activated Carbons: A Sustainable Approach for Dye Removal and Wastewater Treatment

Beatriz Alvez-Tovar [1,2,*], Paulo Sergio Scalize [2], Giovanny Angiolillo-Rodríguez [3], Antonio Albuquerque [4,*], Malorie Ndemengane Ebang [5] and Tatianne Ferreira de Oliveira [6]

[1] Institute of Experimental Biology, Faculty of Sciences, Central University of Venezuela-UCV, University City of Caracas, Capital District, Caracas 47604, Venezuela
[2] School of Civil and Environmental Engineering, Federal University of Goiás-UFG, Colemar-Natal Campus, Goiânia 74690-900, Goiás, Brazil; pscalize.ufg@gmail.com
[3] Postgraduate Program in Agroecology, State University of Maranhão-UEMA, Paulo VI University City, São Luís 65800-000, Maranhão, Brazil; giovanny.angiolillo@gmail.com
[4] GeoBioTec, Civil Engineering and Architecture Department, University of Beira Interior, Fonte Calçada do Lameiro, 6201-001 Covilhã, Portugal
[5] Stricto Sensu Graduate Program in Environmental and Sanitary Engineering (PPGEAS), School of Civil and Environmental Engineering, Federal University of Goiás-UFG, Colemar-Natal Campus, Goiânia 74690-900, Goiás, Brazil; nmalorie@discente.ufg.br
[6] Department of Food Engineering, School of Agronomy, Federal University of Goiás-UFG, Samambaia Campus, Goiânia 74690-900, Goiás, Brazil; tatianne_ferreira_oliveira@ufg.br
* Correspondence: beatriz.alvez@ufg.br (B.A.-T.); antonio.albuquerque@ubi.pt (A.A.)

Abstract: The increasing generation of agro-industrial waste has intensified soil and water contamination, as well as the eutrophication of water bodies, impacting biodiversity and human health. This highlights the need for responsible management to meet Sustainable Development Goals (SDGs) 3, 6, 12, 13, 14, and 15, which promote health, access to clean water, responsible consumption, climate action, and the protection of life on land and below water. This study aimed to produce activated carbon from cocoa, baru, and monguba residues for the removal of contaminants dyes (methylene blue, bromocresol green, and methyl red) presented in wastewater. The three materials were carbonized at 500 °C for one hour under a nitrogen atmosphere and activated with H_3PO_4. The samples were characterized using TGA, SEM, XRD, FT-IR, pH_{PZC}, and ASAP, in addition to conducting kinetic and thermodynamic parameter assays for the dyes. Monguba carbon exhibited the highest pore volume (1.57 $cm^3 \cdot g^{-1}$), surface area (1604 $m^2 \cdot g^{-1}$), and adsorption capacity for methylene blue and methyl red (50 $mg \cdot g^{-1}$). The data were analyzed using pseudo-first and pseudo-second order kinetic models. It was concluded that monguba carbon shows potential for the sustainable removal of organic dyes and molecules with similar characteristics in contaminated water or wastewater.

Keywords: *Theobroma cacao* L.; *Dipterix alata* Vog.; *Pachira aquatica* Aubl.; solution for dye removal; sustainable water treatment; agro-industrial waste management

check for updates

Academic Editors: Slavica S. Lazarević and Ivona Janković-Castvan

Received: 4 January 2025
Revised: 6 February 2025
Accepted: 10 February 2025
Published: 26 February 2025

Citation: Alvez-Tovar, B.; Scalize, P.S.; Angiolillo-Rodríguez, G.; Albuquerque, A.; Ebang, M.N.; de Oliveira, T.F. Agro-Industrial Waste Upcycling into Activated Carbons: A Sustainable Approach for Dye Removal and Wastewater Treatment. *Sustainability* **2025**, *17*, 2036. https://doi.org/10.3390/su17052036

1. Introduction

Technological advances have increased pollutants in the environment and water, with organic dyes being among the most hazardous [1]. The use of dyes is expanding across various industries, such as textiles, paper, plastics, food, and cosmetics, resulting in massive annual production [2]. Up to 15–20% of these dyes are released in wastewater [3], presenting concentrations between 100 and 500 $mg \cdot L^{-1}$ in textile wastewater [4,5]. These dyes

are difficult to treat due to the complexity of their molecular structure, chemical stability, and high resistance to biodegradation, posing risks to both human health and the environment [1]. More than 10% of the dyes produced during industrial processes are resistant to water, sweat, light, oxidizing agents, and microorganisms. Even at concentrations as low as 1 $mg \cdot L^{-1}$ in wastewater, dyes are visible [5], affecting water quality due to color changes and toxicity, posing cancer and mutation risks. This makes wastewater treatment prior to discharge into effluents, in many cases, a higher priority than the removal of other compounds [6].

Methylene blue (MB), classified as a cationic thiazine dye with the Color Index Number CI 52015, is widely used in industries such as textiles, biology, and chemistry due to its water solubility and chemical stability. This dye is particularly employed in the coloring of materials like wool and silk, and it can adsorb onto negatively charged surfaces. Structurally, MB contains a heterocyclic aromatic ring that facilitates strong interactions with adsorbent surfaces, particularly through electrostatic attraction. This property, combined with its high visibility even at low concentrations, makes it an ideal candidate for evaluating adsorption processes. However, MB has adverse effects on human health, such as methemoglobinemia, cyanosis, seizures, tachycardia, eye and skin irritation, digestive disorders, mental confusion, vomiting, anemia, hypertension, and dyspnea. It also affects the metabolism of aquatic organisms and has teratogenic effects on fish [7–12]. Bromocresol green (BCG), a triphenylmethane dye, is commonly used as a pH indicator and coloring agent in analytical and laboratory applications. Unlike other industrial dyes, BCG does not have an assigned Color Index Number, as it is not used in dyeing processes or the textile industry but rather in scientific and educational settings. As an anionic dye, BCG contains a sulfonate group in its structure, which increases its solubility in water and enhances its stability. However, its resistance to biodegradation and complex molecular structure make it challenging to remove from wastewater. In the environment, BCG can persist and disrupt the ecological balance, particularly by reducing photosynthetic rates in aquatic ecosystems. Furthermore, it is capable of causing carcinogenic diseases, ocular damage, and nausea, and it also reduces the photosynthetic rate in the marine environment, creating an ecological imbalance, and emphasizing the need for effective adsorption techniques [13–17]. Methyl red (MR), a monoazo dye with the Color Index Number CI 13020, is highly toxic, difficult to degrade, and widely used in the textile industry and as an acid-base indicator [1,18]. It belongs to the category of acidic dyes and contains an azo (-N=N-) group, which is responsible for its intense color and chemical stability. This group, along with its carboxylic acid functional group, enhances its resistance to biodegradation and contributes to its persistence in the environment. MR has been reported to cause irritation to the eyes, skin, and digestive tract in humans, as well as exhibiting mutagenic and carcinogenic effects. It has also been observed that it reduces light penetration into the lower layers of water bodies, decreasing the photosynthetic rate and the oxygen concentration necessary for the survival of aquatic flora and fauna. Within trophic chains, an increase in the concentration of organic dyes has been identified as the chain lengthens, a phenomenon known as bioaccumulation [19–22].

Various methods exist for treating and decolorizing contaminated effluents, such as coagulation, flocculation, photocatalysis, membrane separation, chemical oxidation, ozonation, ion exchange, ultrafiltration, adsorption, and solvent extraction [3,7,23], which often may require membranes, large amounts of energy, and specialized labor. Among these, adsorption stands out for its low cost and high efficiency in removing dyes without generating harmful substances or residues [1]. However, the cost of adsorbents limits their large-scale application. Therefore, it is crucial to identify adsorbents with high adsorption capacity, low production cost, and simple, eco-friendly preparation methods [1,7,24]. Biomass-based adsorbents are promising due to their effectiveness in water treatment and their potential to reduce agro-industrial waste [25–32]. Such biomass can come from various sources, including wood,

agricultural and forestry residues, and crustacean shells [2,33–36]. For instance, activated carbons derived from cocoa shells have been used as adsorbents for contaminants [1,37–39].

Few studies have investigated the production of activated carbon from baru and monguba residues, though promising results have been shown in the adsorption of mercury, nickel, and cadmium [40,41] or in improving post-harvest food storage conditions [42]. Other agro-industrial residues have been transformed into activated carbon to remove MB, BCG, and MR, highlighting the importance of treating wastewater containing these dyes [7,11,43–45]. Cocoa (*Theobroma cacao* L.), baru (*Dipteryx alata* Vog.), and monguba (*Pachira aquatica* Aubl.) are valuable tropical trees known for their fruits, but they also generate waste. Cocoa seeds, essential for chocolate production, have shells that are often discarded [46,47]. Baru and monguba fruits are highly nutritious; however, the residues generated during seed extraction are considerable [26,48,49]. Utilizing these residues to produce activated carbon could help mitigate environmental pollution while contributing to food security and local economies [50–52].

In this context, the novelty presented in this work is two-fold: the utilization of cacao, baru, and monguba shells, which reduces the amount of waste in the environment and promotes their circularity, thereby adding value to these materials; moreover, the demonstration of the potential of activated carbons derived from these residues as adsorbents for the removal of dyes from wastewater and drinking water. Furthermore, the valorization of these residues into activated carbons supports a circular economy by ensuring they are reused instead of discarded, reducing environmental impact and promoting sustainability. The cacao, baru, and monguba residues are low-cost and widely available in Brazil and other countries where these plants are cultivated, making them accessible to both urban and rural communities. The low production costs of these adsorbents could also lead to cost-effective solutions for wastewater and drinking water treatment, contributing to efficient water resource management in various regions. The selection of MB, BCG, and MR as model dyes for this study reflects their environmental relevance, chemical diversity, industrial significance, and toxicity. MB represents cationic dyes, BCG illustrates anionic triphenylmethane dyes, and MR exemplifies monoazo dyes, providing a comprehensive understanding of the adsorption potential of activated carbons derived from cacao, baru, and monguba shells. Furthermore, the use of these dyes allows for visual monitoring of the adsorption process, as they can be visualized at low concentrations, making them ideal for evaluating adsorption effectiveness. Although studies on the activation of cacao and baru carbons with H_3PO_4 already exist, the experimental conditions used in this work, such as temperature and activation time, differ, allowing for the exploration of new characteristics and adsorption capacities and providing a physicochemical interpretation of the adsorption mechanisms of these alternative materials.

This research contributes to the circular economy by upcycling cacao, baru, and monguba residues into valuable activated carbon, addressing the growing need for sustainable wastewater treatment. By utilizing agro-industrial waste, this study not only offers an eco-friendly solution to environmental pollution but also promotes responsible consumption and production. Moreover, it directly contributes to several Sustainable Development Goals (SDGs), including SDGs 3 (Good Health and Well-being), 6 (Clean Water and Sanitation), 12 (Responsible Consumption and Production), 13 (Climate Action), 14 (Life Below Water), and 15 (Life on Land). The results of this study further complement previous research on activated carbon from cacao and baru, while introducing new activation conditions and providing valuable insights into the adsorption potential of these materials.

2. Materials and Methods

2.1. Chemicals

Orthophosphoric acid (H_3PO_4) 85% PA (CAS 7664-38-2), Hydrochloric acid (HCl) 37% PA ACS (CAS 7647-01-0), and Sodium hydroxide microbeads (NaOH) PA (CAS

1310-73-2) from Neon Comercial Reagentes Analíticos LTDA, Suzano, SP, Brazil; Granulated activated carbon (CAS 7440-44-0) and Sodium chloride (NaCl) PA (CAS 7647-14-5) from Dinâmica Química Contemporanea LTDA, Indaiatuba, SP, Brazil.; Methylene blue ($C_{16}H_{18}CIN_3S{\cdot}3H_2O$) PA (CAS 122965-43-9), Bromocresol green ($C_{21}H_{14}Br_4O_5S$) PA ACS (CAS 76-60-8) and Methyl red ($C_{15}H_{15}N_3O_2$) PA ACS (CAS 493-52-7), from Qhemis Hexis Científica, Jundiaí, SP, Brazil. In Table 1, the properties of the dyes that serve as adsorbates in the study can be observed.

Table 1. Characteristics of dyes [12,17,22]. The light blue, red, dark blue, yellow, light green, dark green, and white balls represent carbon, oxygen, nitrogen, sulfur, chlorine, bromine, and hydrogen atoms, respectively.

Properties	Methylene Blue	Bromocresol Green	Methyl Red
IUPAC Name	[7-(dimethylamine)phenothiazin-3-ylidene]-dimethylazanium;chloride	2,6-dibromo-4-[3-(3,5-dibromo-4-hydroxy-2-methylphenyl)-1,1-dioxo-2,1λ^6-benzoxathiol-3-yl]-3-methylphenol	2-[[4-(dimethylamine)phenyl]diazinyl]benzoic acid
Chemical Structure Model by ChemSketch (Freeware), version 2023.2.4: ACD/Labs, Toronto, ON, Canada. 4 February 2024 [53]	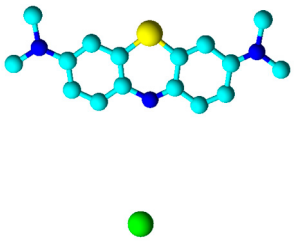	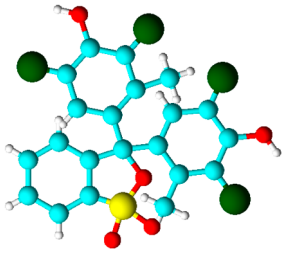	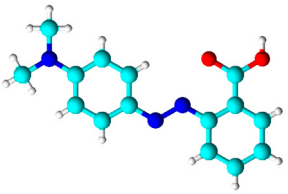
Molecular formula	$C_{16}H_{18}ClN_3S$	$C_{21}H_{14}Br_4O_5S$	$C_{15}H_{15}N_3O_2$
Molecular dimension	1.6–2.0 nm	1.8–2.2 nm	1.3–1.5 nm
Molecular Weight	319.9 g·mol^{-1}	698.0 g·mol^{-1}	269.30 g·mol^{-1}
Dissociation Constant pKa (25 °C)	3.80	4.51	4.82
Chemical Safety	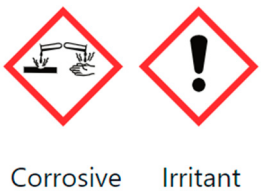 Corrosive Irritant	 Irritant	 Health Hazard Environmental Hazard

Spheres represent the following elements: Carbon (C) in cyan, Hydrogen (H) in white, Oxygen (O) in red, Nitrogen (N) in blue, Chlorine (Cl) in light green, Sulfur (S) in yellow, and Bromine (Br) in green.

2.2. Samples

As precursor materials for the activated carbons produced in this work, cocoa, baru, and monguba shells were used, which come from different regions of Brazil: Ilhéus municipality, Bahia state (cocoa), Várzea da Palma municipality, Minas Gerais state (baru) and Camaçari municipality, Bahia state (monguba). Samples were washed to remove surface dirt and dried at 110 °C for 24 h in an oven (TECNAL, TE-394/3, Piracicaba, SP, Brazil), crushed in a shredder (LIPPEL, TL 1200, Agrolândia, SC, Brazil), and screened at Mesh 2 and stored in a desiccator until use.

2.3. Preparation of Activated Carbons

To obtain activated carbons (CAC: cocoa activated carbon; BAC: baru activated carbon; MAC: monguba activated carbon), we followed the methodologies of Boundzanga et al. [54] and Pereira et al. [55], with modifications, for carbonization and chemical activation. The dried and crushed cocoa, baru, and monguba shells were impregnated with 85% H_3PO_4 activation agent, in a 1:2 ratio (sample:activation agent) and kept at 80 °C under stirring for 60 min at 100 rpm. The samples were filtered with fine mesh (1 mm) for a few seconds and immediately placed in an oven at 110 °C for 24 h. After this time, the samples were

carbonized in a quartz reactor, inside a tubular furnace (SANCHIS, FT 1200, Porto Alegre, RS, Brazil) under the following conditions: 500 °C, with a heating rate of 10 °C min^{-1}, under N_2 flow (160 mL·min^{-1}), for 1 h. After carbonization, the samples were allowed to cool to 25 ± 1 °C and were treated with a wash with 37% HCl to remove ash formed and other impurities generated during the heat treatment. Then, the samples were washed with ultrapure H_2O and 0.01M NaOH until reaching neutral pH. Afterward, the samples were placed in an oven at 110 °C for 24 h to ensure complete evaporation of the water. Finally, the dried activated carbons were stored in a desiccator at 25 ± 1 °C for further studies.

2.4. Characterization of Activated Carbons

2.4.1. Thermogravimetric Analysis (TGA/DTA)

The thermogravimetric analysis was carried out using the Thermogravimetric Analyzer (SHIMADZU, DTG-60H, Kyoto, Japan), which records a weight loss of 1 g of coal as a function of temperature under specific and controlled conditions: 0 to 800 °C, with a heating rate of 10 °C min^{-1}, under the influence of N_2 atmosphere (50 mL·min^{-1}) [56].

2.4.2. Yield of Produced Activated Carbons

The percentage yield (Y) of the samples was estimated according to Equation (1) [10],

$$Y(\%) = \frac{X_1}{X_o} \times 100 \quad (1)$$

where x_o is the weight of the precursor material (g) and x_1 is the weight of the activated carbon (g).

2.4.3. Scanning Electron Microscopy (SEM)

SEM analyses were carried out using a Scanning Electron Microscope (JEOL, JSM—7100F, Peabody, MA, USA) with the aim of determining the topography of the activated carbon samples. This equipment uses a source from which a beam of electrons comes out with a current of 30 keV and a detector of electrons reflected by the sample [56].

2.4.4. X-Ray Diffraction (XRD)

For qualitative information on the composition of the mineral phase of the carbon, we sample formats subjected to X-ray diffraction (XRD). This instrumental technique generates diffractograms through a diffractometer (BRUKER, D8 Discover, Billerica, MA, USA) by means of monochromatic radiation from a tube with a copper anode coupled to a Johansson monochromator for Kα1 equipped with a radiation source (40 kV, 40 mA), Bragg–Brentano configuration θ–2θ, one-dimensional detector (LYNXEYE®, Billerica, MA, USA), and 2θ range from 5° to 100°, step of 0.01°, keeping the samples in motion at 15 rpm during the measurement [56].

2.4.5. Fourier Transform Infrared Spectroscopy (FT-IR)

For the analysis of the chemical structure of the carbon and identification of functional groups, Fourier transform infrared spectroscopy (FT-IR) was performed using a spectrophotometer (BRUKER, Vertex 70, Billerica, MA, USA). The transmission was carried out on a KBr tablet, with an acquisition range of 4000–400 cm^{-1}, with an average of 32 measurements, with a resolution of 4 cm^{-1} [56].

2.4.6. Point of Zero Charge (pH_{PZC})

The pH_{PZC} was determined using the 11-point method [57], in duplicate. Therefore, 0.05 g of activated carbon was placed in 10 mL of NaCl solution (0.1 mol·L^{-1}), varying the initial pH (pHi) values from 2 to 12, adjusted with 0.1 mol·L^{-1} HCl and 0.1 mol·L^{-1} NaOH solutions (±0.1 pH units). The suspensions were sealed and kept at 25 °C in a refrigerated

shaker incubator SL-223 at a constant speed of 160 rpm, for 24 h. The solutions were filtered through qualitative filter paper, and the final pH (pHf) was measured with a pH meter (TECNOPON, MPA-210, Piracicaba, SP, Brazil) [33,58].

2.4.7. Analyze Superficial Area and Porosity (ASAP)

The evaluation of the specific surface area and porosity was performed through N_2 adsorption–desorption isotherms (−195.85 °C) in a relative pressure range from 3×10^{-6} to 0.99 obtained by using a high-resolution surface area and porosity analyzer (MICROMERITICS, ASAP 2020 PLUS, São Paulo, SP, Brazil). Prior to measurements, all samples underwent pre-treatment: degassed at 250 °C for 24 h under a residual vacuum of at least 2 μmHg to remove volatiles. The specific BET surface area was determined using the Rouquerol BET transform model [59]. The pore size and pore distribution were determined using the methodology of Jagiello [60] from the porosity analyzer (2D-NLDFT Heterogeneous Surface, 255, carbon-N2-77, São Paulo, SP, Brazil) model integrated into the Solution of Adsorption Integral Equation Using Splines (SAIEUS version 3) program. This model was also used for the determination of the surface area and volume of the micropores and mesopores of the material, as well as the average pore width.

2.5. Dye Adsorption Studies

The adsorption capacity of the activated carbons against three dyes, namely, MB, BCG, and MR, was studied. For this purpose, solutions of 100 $mg \cdot L^{-1}$ of each dye were prepared for the assays, and dilutions of 2, 5, 10, 15, 20, 25, and 30 $mg \cdot L^{-1}$ were made to generate calibration curves (See Figures S1–S3 in Supplementary Materials). The concentration of 100 $mg \cdot L^{-1}$ was selected because it is representative of the dye concentrations found in industrial effluents from the textile sector and has been used in other studies [10,11,19,20,43], which facilitates the comparison of results. Additionally, this concentration allows for the evaluation of the adsorbent's efficiency under conditions close to real ones, establishing an appropriate adsorbent-adsorbate ratio for a better visualization of the adsorption kinetics.

The concentrations of the solutions were analyzed using a UV-visible spectrophotometer (HACH, DR 6000, Jundiaí, SP, Brazil) at the wavelength of maximum absorption for each dye, 665 nm for MB, 515 nm for BCG, and 443 nm for MR. The equilibrium adsorption capacities of the dyes (q_e, $mg \cdot g^{-1}$) were calculated for these adsorbents according to the following mass balance in Equation (2).

$$qe = \frac{(Co - Ce)}{m} \times V \quad (2)$$

where Co and Ce are the initial and equilibrium dye concentrations of the adsorption experiment ($mg \cdot L^{-1}$), m is the adsorbent amount (g), and V is the dye solution volume (L).

These assays were carried out in batch mode, using a refrigerated shaker incubator (SOLAB, SL-223, Piracicaba, SP, Brazil), and maintained at a constant speed of 160 rpm and temperature of 25 ± 1 °C. Each experiment used 50 mL of dye solution at an initial concentration of 100 $mg \cdot L^{-1}$, to which 0.1 g of activated carbon was added. The solutions used in the assays were prepared with ultrapure water and reagents with analytical grade P.A. At predetermined time intervals of 1, 2, 3, 4, 5, and 6 h, samples were collected and filtered through qualitative filter paper to analyze the remaining concentration of the dyes.

2.5.1. Adsorption Kinetics

To obtain the kinetic parameters, the dye adsorption data as a function of time were fitted to the pseudo-first-order (Equation (3)) and pseudo-second-order (Equation (4)) models [61].

$$q_t = q_e[1 - exp(k_1 t)] \quad (3)$$

$$q_t = \frac{k_2 q_e^2 t}{1 + k_2 q_e t} \quad (4)$$

where q_e is the amount of solute adsorbed per unit mass of adsorbent ($mg \cdot g^{-1}$); q_t is the amount of solute adsorbed per unit mass of adsorbent ($mg \cdot g^{-1}$) at time t (minutes); k_1 is the kinetic constant of pseudo-first order (min^{-1}); k_2 is the kinetic constant of the pseudo-second-order ($g \cdot mg^{-1} \cdot min^{-1}$) [62].

A multifactorial analysis of variance (ANOVA) was performed using Statgraphics Centurion to evaluate the influence of two main factors: the type of dye (MB, BCG, and MR) and the type of adsorbent material (BAC, CAC, and MAC) on the maximum adsorption capacity (q_{max}). The analysis was conducted using Type III sums of squares, F-tests, and *p*-values, with a 95% confidence level.

2.5.2. Adsorption Thermodynamics

In the final stage of this study, we examined the effect of temperature on the efficiency of organic dye removal. The experiments were conducted at three different temperatures: 298.15, 308.15, and 318.15 K. Adsorption experiments involving aqueous solutions of organic dyes on CAC, BAC, and MAC were carried out for a duration of 6 h. The samples were agitated at a shaking speed of 160 rpm, using 0.1 g of activated carbon and a dye concentration of 50 $mg \cdot L^{-1}$ for MB, BCG, and MR. The values of q_e at 60, 180, and 360 min were determined using Equation (2). The thermodynamic parameters, including ΔG (standard Gibbs free energy), ΔH (enthalpy change), and ΔS (entropy change), were calculated based on Equations (5)–(8):

$$Kd = \frac{qe}{Ce} \quad (5)$$

$$\Delta G = -RTlnKd \quad (6)$$

$$\Delta G = \Delta H - T\Delta S \quad (7)$$

$$lnKd = \frac{\Delta S}{R} - \frac{\Delta H}{RT} \quad (8)$$

where ΔG is the Gibbs free energy ($kJ \cdot mol^{-1}$), R represents the gas constant (8.314 $J \cdot mol^{-1} \cdot K$), T is the temperature (K), Kd refers to the thermodynamic equilibrium constant and represents the ratio of the concentration of adsorbate in the solid phase (adsorbent) to its concentration in the liquid phase (adsorbate), at equilibrium, and is used to evaluate the tendency of the adsorbent to retain or release the contaminant, while ΔH ($J \cdot mol^{-1}$) is the enthalpy change, and ΔS ($J \cdot mol^{-1} \cdot K$) is the entropy change [20,35]. To calculate ΔH and ΔS, we plotted lnKd against T^{-1}, resulting in a graph known as the Van 't Hoff plot [63,64].

3. Results and Discussion

3.1. Characterization of Activated Carbons

3.1.1. Thermogravimetric Analysis (TGA/DTA)

The thermogravimetric analysis (TGA) of the precursor materials provided crucial information for selecting the optimal carbonization temperature. This step was essential to ensure favorable carbonization conditions and sufficient material recovery for subsequent experiments. The TGA/DTA profiles, showing the thermal behavior of cocoa, baru, and monguba residues prior to the carbonization process, were plotted as mass loss as a function of temperature and are presented in Figure 1.

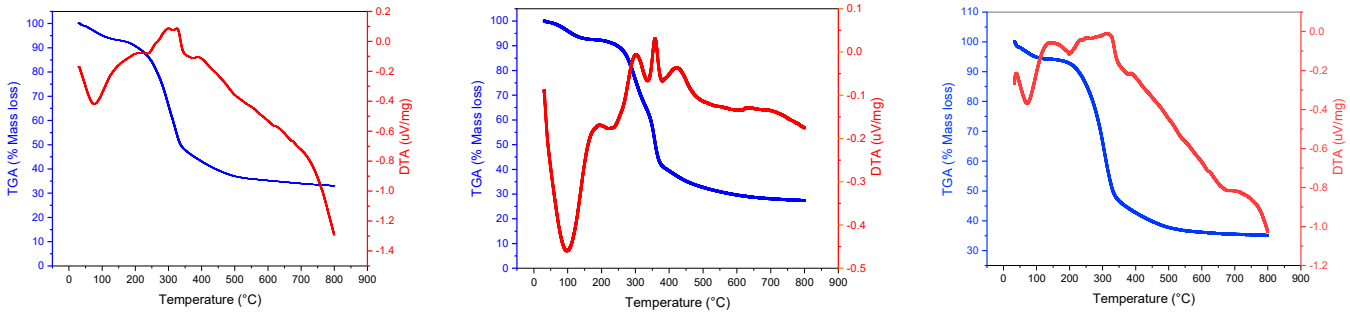

(**a**) (**b**) (**c**)

Figure 1. Thermogravimetric analysis of (**a**) cocoa, (**b**) baru, and (**c**) monguba before carbonization. The blue line (TGA) represents the percentage of mass loss of the untreated materials as a function of increasing temperature; the red line (DTG) represents the derivative of TGA.

The thermogravimetric analyses of cocoa, baru, and monguba residues revealed mass loss events prior to carbonization: water evaporation (~80–120 °C), hemicellulose degradation (~200–350 °C), cellulose (~270–410 °C), and lignin (~200–500 °C), similar to other agro-industrial residues [65–69]. No significant mass loss was observed beyond 500 °C, indicating that complete decomposition occurred at this temperature. Therefore, carbonization at 500 °C was selected, with an expected material recovery of approximately 30%.

After the carbonization and activation process, the TGA/DTA results were verified. As shown in Figure 2, the obtained materials demonstrated thermal resistance at 500 °C, evidenced by low mass loss values, with a maximum of 26.37% for baru and a minimum of 10.74% for monguba (Table 2). These results exhibited a trend similar to those observed for other plant residues [70–72].

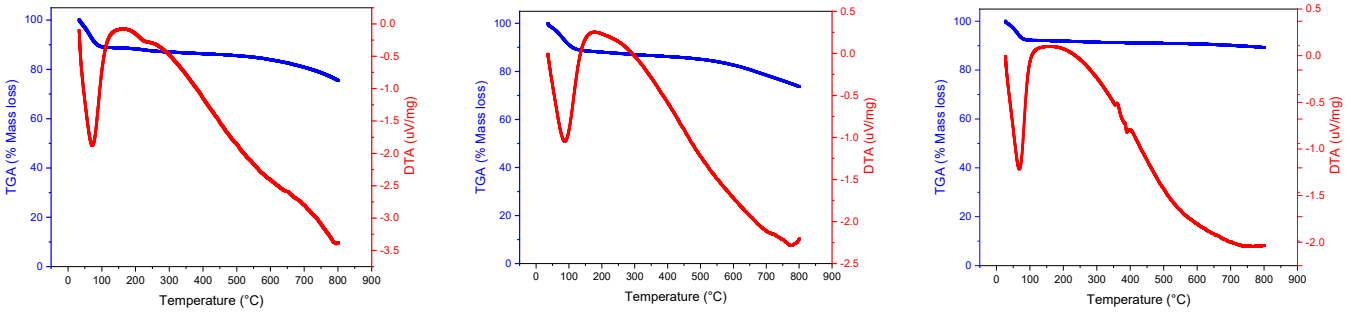

(**a**) (**b**) (**c**)

Figure 2. Thermogravimetric analysis of: (**a**) CAC; (**b**) BAC; (**c**) MAC. The blue lines represent the percentage of mass loss (TGA) of the activated carbons as a function of increasing temperature, and the red lines represent the derivative of TGA (DTA).

Table 2. Evaluation of the % total mass loss of carbonized materials.

Material	Initial Weight (mg)	Initial Mass (%)	Final Weight (mg)	Final Mass (%)	Mass Loss (%)
CAC	10.13	100	7.64	75.40	24.60
BAC	12.976	100	9.55	73.63	26.37
MAC	13.17	100	11.75	89.26	10.74

3.1.2. Yield of Produced Activated Carbons

After the carbonization and activation processes, materials were recovered that maintained their granular integrity, with a yield ranging from 30.00% to 36.70% (Table 3). This similarity is attributed to the comparable chemical composition of the species, which are rich

in cellulose, hemicellulose, and lignin. These compounds thermally decompose during carbonization, forming a carbonaceous matrix. Lignin, the most resistant compound, contributes to the charcoal yield, demonstrating that these materials are excellent precursors for activated carbon production [10,73].

Table 3. Yield of carbonized materials.

Precursor Material	Yield (%)
Cocoa	36.65
Baru	36.70
Monguba	30.00

3.1.3. Scanning Electron Microscopy (SEM)

In Figure 3, SEM micrographs of the activated carbons are shown at 500× magnification with a scale bar of 10 µm. In general, irregular surfaces and pore formation can be observed in the micrographs. For CAC, a well-developed porous structure with relatively uniform pore sizes is noted, similar to the results of previous studies [74].

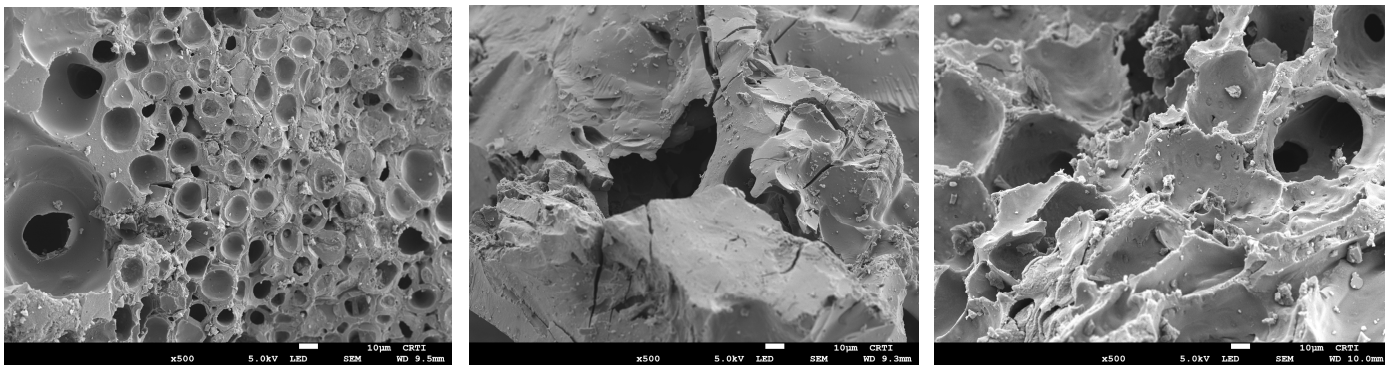

(**a**) (**b**) (**c**)

Figure 3. SEM Images with 500× magnification of the activated carbons from (**a**) CAC; (**b**) BAC; (**c**) MAC.

Activation with H_3PO_4 appears to have created a homogeneous pore network, ideal for applications requiring a high specific surface area. Chemical impregnation, by promoting cross-linking formation, leads to the development of a rigid porous matrix. Furthermore, biomass chemically activated with acid or base prior to pyrolysis oxidizes the porous carbon surface, enhancing its acidity and removing mineral elements, which also improves the hydrophilicity of the adsorbent surface [8].

BAC exhibits a less uniform structure compared to cocoa, with visible fractures and cracks, indicating that the chemical activation process affected the morphology of baru differently. In MAC, the porous structure is well-defined, similar to cocoa, although with more variable pore sizes, which may be beneficial for certain types of adsorption that require a range of pore sizes [62,73,75].

3.1.4. X-Ray Diffraction (XRD)

X-ray diffraction analysis complemented the structural analysis of the activated carbons (Figure 4). It is observed that the materials have a high carbon content, indicative of adsorbent materials. Additionally, broad peaks are visible in the 2θ range between 10° and 30°, indicating a predominant amorphous structure. This characteristic is typical of chemically activated carbons, where activation with H_3PO_4 promotes the formation of a porous network by reducing the crystallinity of the original material [7,42,76].

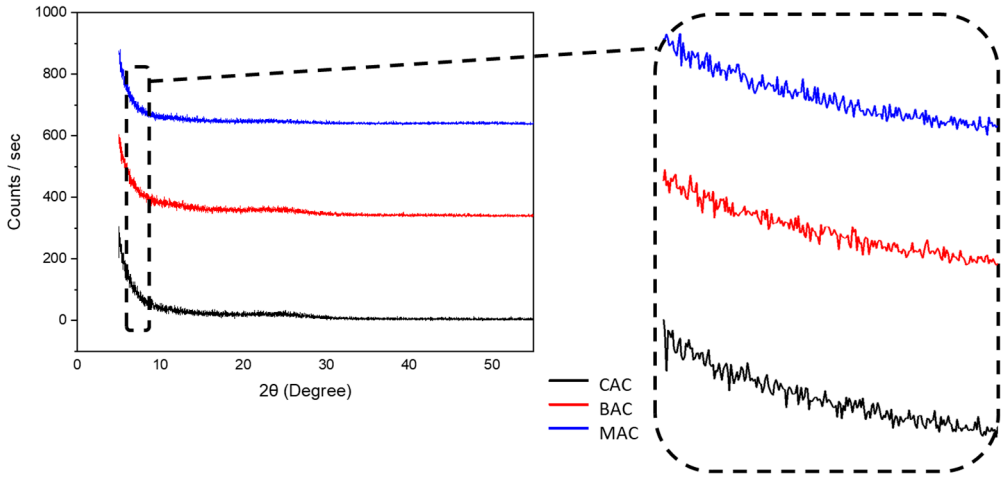

Figure 4. X-ray diffractograms (XRD) of CAC (black line); BAC (red line); MAC (blue line).

3.1.5. Fourier Transform Infrared Spectroscopy (FT-IR)

The FT-IR spectra of the carbons show characteristic bands for functional groups (Figure 5). There is a broad band between 3700–3000 cm^{-1}, indicating hydroxyl groups (O-H); a peak between 1700–1600 cm^{-1}, suggesting carbonyl groups (C=O); and smaller bands between 1400–1000 cm^{-1}, associated with phosphate groups (P=O, P-OH, P-O-C) introduced by H_3PO_4. These bands indicate a high presence of oxygenated functional groups, which improve the interaction between the adsorbent and the adsorbates. The treatment with H_3PO_4 introduces phosphate groups and modifies the chemical structure, increasing the number of acidic groups such as -OH and -COOH, and depolymerizing components like lignin and cellulose [8].

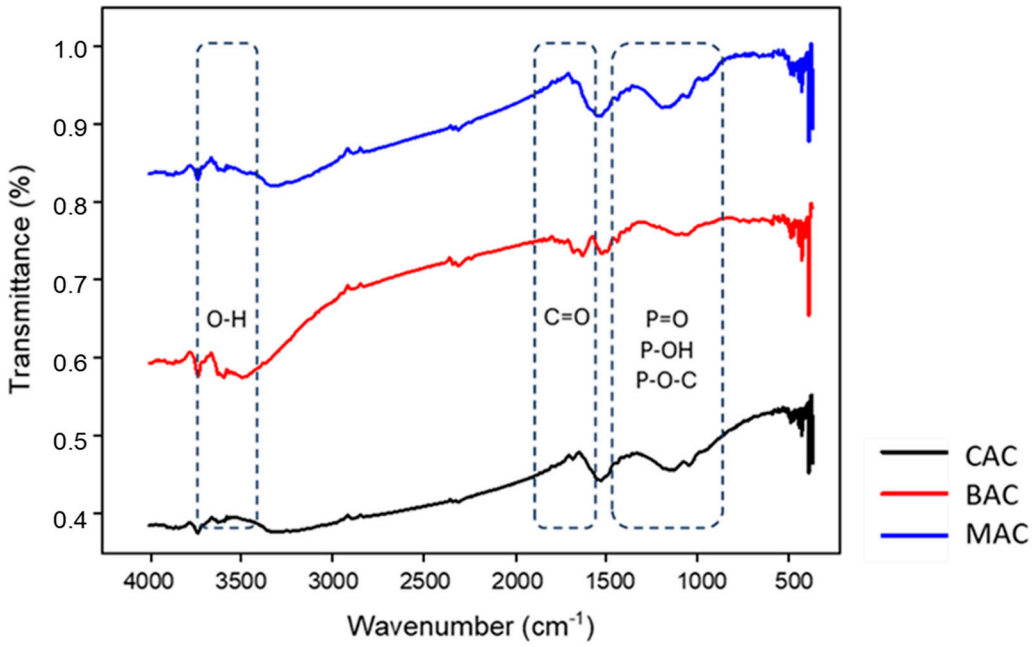

Figure 5. FT-IR spectrum of CAC (black line); BAC (red line); MAC (blue line).

In previous studies, it has been reported that the surface of acid-treated oxidized carbon develops more negatively charged species compared to conventional activated carbon, due to the dissociation of acidic functional groups on its surface, which enhances the electrostatic interaction between the adsorbent and the adsorbate. An example of this is the study by Patel et al. [8], in which activated carbon prepared from wood biomass, impregnated with

different agents such as H_3PO_4, $ZnCl_2$, KOH, and CaO for dye removal, showed that the highest adsorption capacity for dyes like Rhodamine B and Methylene Blue is achieved with activation using H_3PO_4. Table 4 compares the functional groups found after the treatment with H_3PO_4 in the carbons obtained in this study with those from another research.

Table 4. Functional groups introduced in carbons activated with H_3PO_4.

H_3PO_4-Activated Carbon	Functionals Groups	References
Cocoa shells	OH, C=O, P=O, P-OH, P-O-C	This work
Baru shells	OH, C=O, P=O, P-OH, P-O-C	This work
Monguba shells	OH, C=O, P=O, P-OH, P-O-C	This work
Fruits shells	OH, CH, C=O, P=O, C–O, P-O-C, P=OOH, P-O-P, P-H, C-P	[77]
Jackfruit peel	OH, CH, C=O, C=C, P=O, C–O, P-O-C, P=OOH, P-O-P	[65]
Pineapple leaf	OH, CH, C=O, C=C, P=O, C–O, P-O-C, P=OOH, P-OH, P-C, PO_2, PO_3	[78]
Jujube seeds	OH, CH, C=O, C=C, P-O-P	[63]
Lemon shells	OH, CH, C–O, COO, C=C, C=O	[43]
Olive stone	OH, CH, P-O, P-O-C, C–O	[9]

The functional groups observed in the carbons in Table 4 are typical of lignocellulosic materials subjected to an acid pre-treatment at high temperatures, where phosphorus oxides act as Lewis acids and can create –P-O-C bonds. These studies confirm the effectiveness of H_3PO_4 in introducing phosphate groups and other oxygenated functional groups, which improves the adsorption properties of the activated carbons [8,9,43,63].

3.1.6. Point of Zero Charge (pH_{PZC})

The pH_{PZC} was determined from the ΔpH (=pHf − pHi) versus pHi graph (Figure 6). When the pH is below the pH_{PZC}, the surface of the adsorbent is positively charged, favoring the adsorption of anions. On the other hand, if the pH is above the pH_{PZC}, the surface acquires a negative charge, facilitating the adsorption of cations [36,56,58].

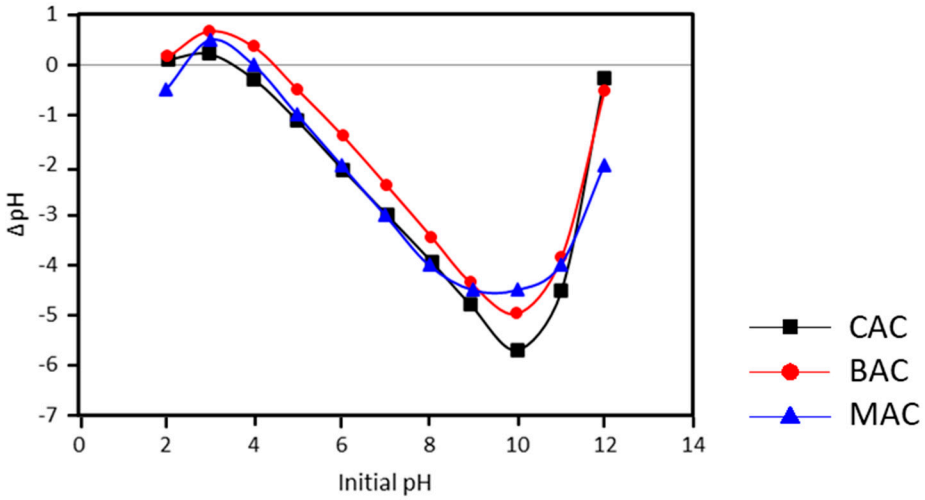

Figure 6. Point of zero charge (pH_{PZC}) analysis from CAC, BAC, and MAC.

The intersection of the curve with the horizontal axis (where ΔpH is zero) indicates the point of zero charge (pH_{PZC}). For CAC, the pH_{PZC} is around an initial pH of 3.8, meaning that at a pH below this value, the charcoal surface is positively charged, while at a pH above this value, it acquires a negative charge. In the case of BAC, the intersection with the horizontal

axis occurs at an initial pH of approximately 4.6, indicating that its pH_{PZC} is around this value. At a lower pH, the surface will be positively charged, and at a higher pH, it will be negatively charged. Since the pH of the solution influences the charge on the adsorbent surface and the ionization state of the dyes, it plays a crucial role in the adsorption process. A systematic evaluation of the effect of pH could provide further insights into the interactions between the adsorbent and adsorbates, which is an area for potential future research. For MAC, the pH_{PZC} is observed at an initial pH close to 4.2, which implies that, at lower pH values, the surface is positively charged, while at a pH above this value, it is negatively charged.

The activation with H_3PO_4 generates an acidic carbon surface [71], which can influence its adsorption behavior depending on the pH of the solution and the chemical behavior of each dye. The adsorption of MB, which is cationic in nature, was favored by the negatively charged surface of all three carbons (CAC, BAC, and MAC), resulting in a high adsorption capacity, especially for MAC. On the other hand, the BCG and MR dyes, both anionic in nature, showed more limited adsorption due to electrostatic repulsion between the negatively charged surfaces of the carbons and the anions of the dyes, with this limitation being more pronounced for BAC. Although MAC also shows repulsion, it displayed a slight superiority in adsorbing the anionic dyes, possibly due to textural or chemical characteristics that favor slightly higher adsorption [3,58,79].

The results obtained from SEM, FT-IR, and pH_{PZC} techniques show that activation with H_3PO_4 introduces functional groups on the carbon surface, significantly improving their adsorption properties, especially for cationic dyes such as MB. This process not only alters the surface charge of the carbons but also promotes the creation of active sites essential for the selective adsorption of contaminants based on their charge and chemical nature. The acidic surface resulting from the activation with H_3PO_4 contributes to the observed adsorption behavior, especially in the differences between cationic and anionic dyes [63].

However, despite the positive results in terms of improving surface properties, it is important to consider some limitations and challenges associated with the use of phosphoric acid in the activation process. In particular, activation with H_3PO_4 may have an environmental impact, primarily due to greenhouse gas emissions and the potential release of pollutants during carbonization. Although this activating agent is less toxic compared to others [63,80], research continues to search for more sustainable alternatives that offer porous materials with similar characteristics but with a lower environmental impact [8,19,55]. This challenge highlights the need to continue exploring more eco-friendly approaches in the future without compromising the quality of the active surface required for efficient adsorption.

Considering this, the following section presents the results of the ASAP analysis, which provides additional information on the textural characteristics of the activated carbons and their relationship with adsorption capacity.

3.1.7. Analyze Superficial Area and Porosity (ASAP)

The textural analysis of the activated carbons shows that MAC has the highest specific surface area (SBET) of 1604 $m^2 \cdot g^{-1}$ and the largest total pore volume (1.57 $cm^3 \cdot g^{-1}$). It also has the highest number of mesopores (474 $m^2 \cdot g^{-1}$) and the largest mesopore volume (1.19 $cm^3 \cdot g^{-1}$), with an average pore size of 1.28 nm. This suggests a high adsorption capacity, making it suitable for adsorbing molecules between 2 and 50 nm.

CAC stands out for having the largest microporous surface area (846 $m^2 \cdot g^{-1}$), with an average pore size of 1.14 nm, making it ideal for adsorbing molecules up to 2 nm. BAC has the highest submicroporous surface area (588 $m^2 \cdot g^{-1}$) and an average pore size of 1.19 nm; however, its total pore volume is the lowest (0.70 $cm^3 \cdot g^{-1}$). Table 5 provides detailed information on the textural properties of CAC, BAC, and MAC treated with H_3PO_4.

Table 5. Textural analysis of CAC; BAC; MAC.

Material	CAC	BAC	MAC
S_{BET} ($m^2 \cdot g^{-1}$)	1367	1326	1604
S_T ($m^2 \cdot g^{-1}$)	1134	1007	1163
S_{mic} ($m^2 \cdot g^{-1}$)	846	823	688
S_{meso} ($m^2 \cdot g^{-1}$)	289	184	474
S_{supmic} ($m^2 \cdot g^{-1}$)	503	588	516
S_{umic} ($m^2 \cdot g^{-1}$)	343	235	172
V_T ($cm^3 \cdot g^{-1}$)	1.17	0.70	1.57
V_{mic} ($cm^3 \cdot g^{-1}$)	0.40	0.42	0.38
V_{meso} ($cm^3 \cdot g^{-1}$)	0.77	0.29	1.19
V_{supmic} ($cm^3 \cdot g^{-1}$)	0.30	0.35	0.33
V_{umic} ($cm^3 \cdot g^{-1}$)	0.09	0.07	0.05
L_0 (dV) (nm)	1.14	1.19	1.28

According to the IUPAC classification [81–84], the isothermal profile obtained for the baru charcoal corresponds to type I (Figure 7b), while the cacao and monguba charcoals present a profile more consistent with type II (Figure 7a,c). According to IUPAC classification, type I isotherms approach a limiting value and are generally used to describe adsorption in microporous adsorbents. Types II and III describe adsorption in mesoporous adsorbents with strong and weak adsorbate-adsorbent interactions, respectively. Types IV and V represent mono and multilayer adsorption, while type VI illustrates isotherms that may have one or more steps. For liquid-phase applications, such as dye adsorption, organic acids, and other macromolecules, the development of mesoporous materials is more desirable [43,85]. This fact is corroborated by the results of this study, where CAC and MAC show higher efficiency in adsorption compared to BAC.

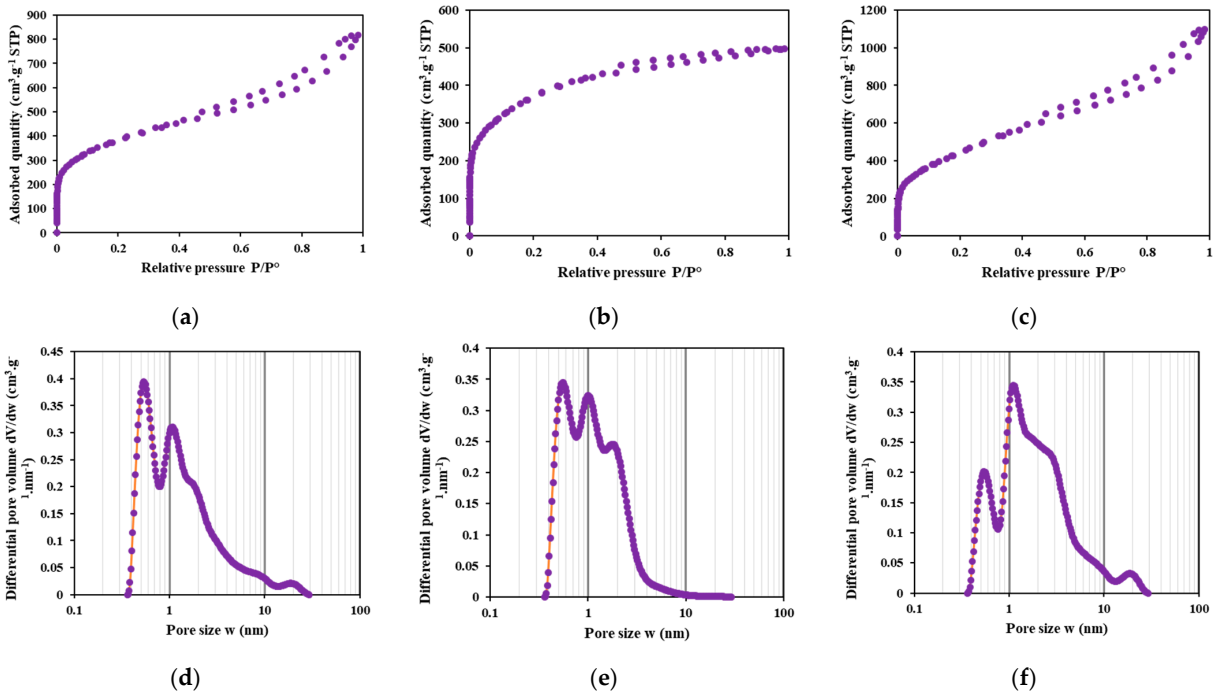

Figure 7. Nitrogen adsorption–desorption isotherm curves of (**a**) CAC; (**b**) BAC; (**c**) MAC; and pore size distribution curves of (**d**) CAC; (**e**) BAC; (**f**) MAC.

In summary, MAC is the most suitable for applications requiring high adsorption capacity due to its large surface area and pore volume, CAC can adsorb smaller molecules up to 2 nm. In the case of BAC, further tests under different carbonization conditions are needed to obtain a material with greater surface area and pore volume.

3.2. Dye Adsorption Studies

3.2.1. Adsorption Kinetics

The kinetic study of adsorption is important for predicting the optimal conditions in batch adsorption, providing valuable information about the adsorption mechanisms and the potential steps that control the rate [21]. Physisorption is characterized by weak physical interactions (Van der Waals forces) and is typically described by the pseudo-first-order kinetic model. This model assumes that the rate of occupation of adsorption sites is proportional to the number of unoccupied sites [36,86]. On the other hand, chemisorption involves stronger chemical bonds between the adsorbate and the adsorbent. It is described by the pseudo-second-order kinetic model, which assumes that the adsorption rate is proportional to the square of the number of unoccupied sites, indicating more specific and energetically intense interactions. When activation is carried out with H_3PO_4, functional groups are introduced on the surface of the charcoal, which may favor chemisorption due to specific chemical interactions between the adsorbates and the active sites on the activated carbon surface [87,88]. Figure 8 shows the results of the adsorption kinetics of the activated carbons in relation to the MB, BCG, and MR dyes.

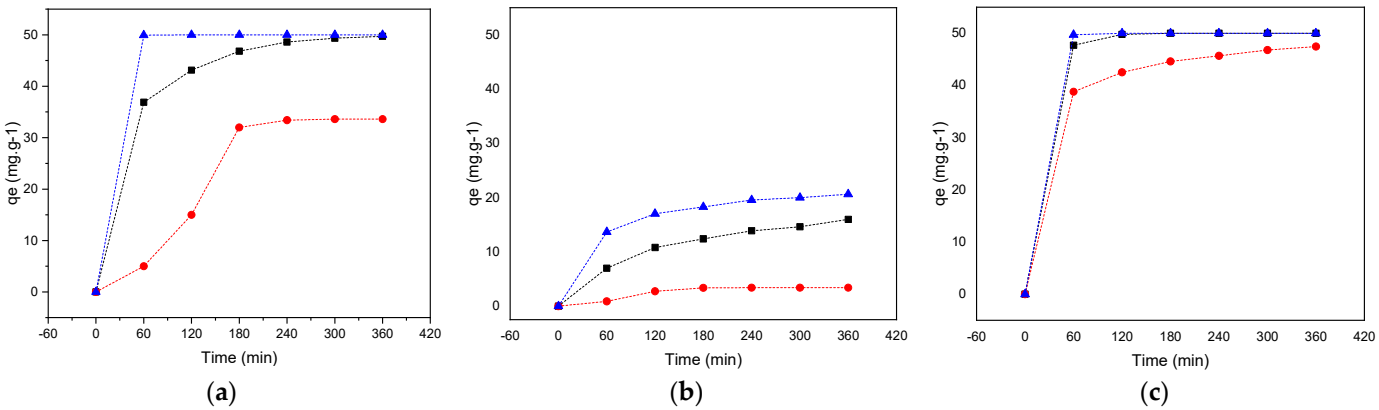

Figure 8. Adsorption kinetics of (**a**) MB; (**b**) BCG; (**c**) MR. In all three cases: CAC (dash black line), BAC (dash red line), and MAC (dash blue line).

The three activated carbons showed differences in their adsorption capacity. Monguba charcoal stood out for its high capacity (50.00 $mg \cdot g^{-1}$), reaching equilibrium for most of the dyes before 60 min.

The CAC, although effective for MB and MR (49.52 and 50.00 $mg \cdot g^{-1}$, respectively), was slightly less effective than the MAC, especially for BCG (15.31 $mg \cdot g^{-1}$), possibly due to the characteristics of the dye. The BAC showed the lowest adsorption capacity for all the dyes, which could be related to its porous structure or surface nature. Factors such as functional groups and pore size influence the adsorption process [19,66].

A preliminary comparison with commercial activated carbon for the adsorption of the three dyes is provided in the Supplementary Materials (Figure S5). The results indicate that while the commercial carbon exhibits better adsorption capacity for MB, the adsorption capacities are similar to those of the BAC, and the CAC and MAC demonstrate higher capacities, highlighting their potential as competitive materials.

In MB adsorption, equilibrium was reached at 60 min, indicating the high affinity of the three carbons for this dye, possibly due to its molecular size. It is necessary to perform

readings at times shorter than 60 min to evaluate more precisely when the adsorption process begins. In Figure S4 (Supplementary Materials), the color reduction resulting from the adsorption process performed using the MAC for MB can be observed, evidencing solution clarification as proof of the adsorption process. In the case of BCG, the adsorption gradually stabilized, suggesting a less favorable interaction compared to MB [13,89,90]. MR adsorption was rapid but stabilized more slowly [19,91,92]. Differences between the dyes may be related to molecular size, polarity, or structure, with MB and MR being adsorbed more easily; however, BCG, due to its more complex structure, has limited adsorption [20,90,92]. The adsorption kinetics initially followed a fast pattern, slowing down over time as the more accessible sites were exhausted [8,19,90].

The pseudo-first-order model is based on the fact that the adsorption rate is proportional to the number of available adsorption sites on the adsorbent surface [36]. The pseudo-second-order model assumes that the adsorption follows a chemical exchange mechanism, where the adsorption rate is proportional to the square of the number of available sites [20,88]. The results of fitting the pseudo-first-order and pseudo-second-order kinetic models suggest that the adsorption process is controlled by chemical interactions between the adsorbents and the dyes, especially for MB and MR, which is consistent with the behavior observed in the studied systems, particularly those with fast initial adsorption and higher final adsorption capacity (CAC and MAC). This result is similar to that obtained by Chen et al. [93], where the experimental data showed a better fit to the pseudo-second-order model, indicating the existence of partial chemical adsorption through electron exchange between the dyes and the adsorbents.

Based on the data presented in Table 6, a detailed comparison of the kinetic parameters obtained for different dyes and activated carbons can be made. In general, the correlation coefficients (R^2) for the pseudo-first-order model are lower than those for the pseudo-second-order model, suggesting that the first model is not suitable for describing the adsorption kinetic data [9,93,94]. For the MB dye, CAC shows a good fit with an R^2 of 0.983, although the kinetic constant k_1 is negative, indicating possible inconsistencies. BAC and MAC show weaker fits, especially MAC with an R^2 of 0.429. In the case of the BCG dye, the fit is limited, with an R^2 of 0.570 for CAC and better results for MAC (R^2 of 0.99), although the k_1 constants remain negative, suggesting that the model is not appropriate. For the MR dye, MAC shows an excellent fit with an R^2 of 1, while CAC also shows a good fit (R^2 of 0.993); however, BAC has a moderate correlation (R^2 of 0.957). This indicates that the pseudo-first-order model is not the most suitable for most cases due to the low correlation values.

Table 6. Adsorption kinetics parameters of MB, BCG, and MR for CAC, BAC, and MAC (Dyes = 100 mg·L^{-1}; Activated carbons = 0.1 g; pH = 7; Volume = 50 mL; Time = 360 min; Temp. = 25 °C).

Dye	Material	Pseudo-First-Order			Pseudo-Second-Order			q_{max} (mg·g^{-1})
		k_1 (min^{-1})	R^2	q_e (mg·g^{-1})	k_2 (g·mg^{-1}·min^{-1})	R^2	q_e (mg·g^{-1})	
MB	CAC	−0.018	0.983	48.299	0.001	0.999	53.763	49.518
	BAC	−0.0257	0.767	92.444	0.206	0.494	−0.016	33.615
	MAC	0.006	0.429	0.169	0.036	1.000	50.000	50.000
BCG	CAC	−0.014	0.570	34.522	0.000	0.996	20.877	15.315
	BAC	−0.025	0.868	6.336	0.008	0.990	3.788	3.407
	MAC	−0.013	0.990	17.846	0.001	0.999	22.936	20.315
MR	CAC	−0.045	0.993	43.908	0.009	1.000	50.505	50.000
	BAC	−0.015	0.957	32.082	0.001	0.999	49.751	47.115
	MAC	−0.086	1.000	49.999	0.085	1.000	50.000	50.000

The multifactorial analysis of variance conducted to evaluate the effects of the dyes (MB, BCG, and MR) and materials (BAC, CAC, and MAC) on the maximum adsorption capacity (q_{max}) showed statistically significant results. The main factors, dye and material, explained a substantial portion of the variability in q_{max}, with F-values of 59.95 and 6.60, respectively. The dye factor exhibited a *p*-value of 0.0010, indicating a highly significant influence on q_{max}. On the other hand, the material factor obtained a *p*-value of 0.0541, close to the significance threshold (0.05), suggesting a less pronounced but still relevant effect.

The multiple range tests revealed significant differences among the q_{max} means of the dyes evaluated, with methyl red (MR) showing the highest adsorption capacity, followed by methylene blue (MB) and bromocresol green (BCG). Regarding the materials, although no significant differences were observed between them, MAC recorded the highest average q_{max} value, followed by CAC and BAC. This analysis provides robust evidence to conclude that the nature of the adsorbate, in this case, the dye, is the most decisive factor in adsorption performance (Table 7).

Table 7. Analysis of variance for q_{max}—type III sums of squares.

Source	Sum of Squares	Df	Mean Square	F-Ratio	*p*-Value
Dye	2303.38	2	1151.69	59.95	0.0010
Material	253.45	2	126.725	6.60	0.0541
Residual	76.85	4	19.21		
Total (Corrected)	2633.68	8			

On the other hand, the pseudo-second-order model provides a much better fit for the adsorption data, with high R^2 values close to or equal to 1. This model suggests that the adsorption follows a chemical exchange kinetic, dominated by the formation of bonds or specific interactions between the adsorbate and the adsorbent. For MB, CAC shows an excellent correlation (R^2 of 0.999) and a theoretical equilibrium adsorption capacity (q_e) of 53.763 $mg \cdot g^{-1}$, close to the experimental values. MAC also shows a perfect fit (R^2 of 1) with a q_e of 50 $mg \cdot g^{-1}$. However, BAC shows a problematic fit, with an R^2 of 0.4936 and a negative q_e value. For BCG, the CAC fit is good (R^2 of 0.9962), although the adsorption capacity (q_e) is lower (20.877 $mg \cdot g^{-1}$). BAC has a good fit (R^2 of 0.990), while MAC reaches an R^2 of 0.9996, confirming that this model adequately describes the adsorption of BCG. For MR, all the carbons show almost perfect fits to the pseudo-second-order model, with R^2 values close to 1 and theoretical adsorption capacities aligned with the experimental data, around 50 $mg \cdot g^{-1}$.

These results suggest that the pseudo-second-order model better describes the adsorption of dyes onto activated carbons, indicating that the kinetics are controlled by chemical interactions, rather than just the availability of surface sites [94]. The high R^2 values for this model support this conclusion, while the parameters of the pseudo-first-order model do not adequately fit the experimental data in most cases. This is consistent with the observation that the adsorption process involves more complex mechanisms, such as the formation of bonds or specific chemical interactions between the adsorbate and the functional groups present in the activated carbons [9,20,88,93–95].

3.2.2. Adsorption Thermodynamics

In this final section, the effects of temperature variations on the adsorption capacity were analyzed, and the calculated thermodynamic parameters were presented. In general, increasing the temperature tends to favor the adsorption capacity of dyes onto activated carbons, resulting in higher values of q_{max} and Kd [20]. This can be attributed to the increased kinetic energy of the adsorbate molecules at higher temperatures, facilitating their diffusion to the surface of the adsorbent and penetration into the pores. Furthermore, the decrease in

the viscosity of the liquid favors the mobility of the dye molecules, contributing to a higher adsorption rate [69].

However, the magnitude of this effect varies among different materials and dyes. While CAC and MAC show an increase in adsorption with temperature, BAC presents a more limited capacity. It was observed that the maximum adsorption capacity for the three dyes, especially MB, was higher for MAC, reaching between 49.75 and 50 $mg \cdot g^{-1}$, indicating good adsorption properties over a wide range of temperatures. On the other hand, CAC, although reaching values close to 49.8 $mg \cdot g^{-1}$ for all three dyes, showed only 15.32 $mg \cdot g^{-1}$ for BCG at 25 °C (Figure 9).

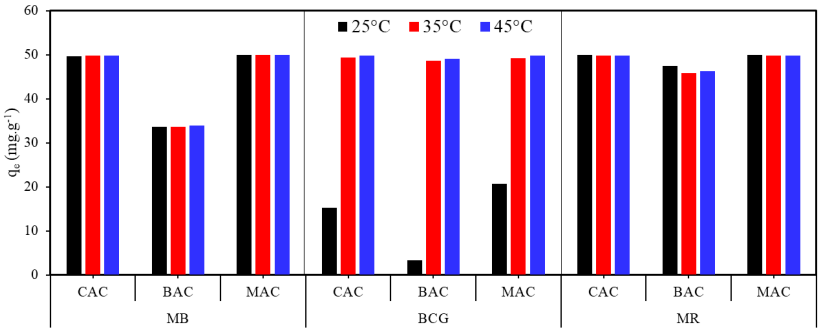

Figure 9. Influence of temperature on the adsorption capacity (q_e) of MB, BCG, and MR, for CAC, BAC, and MAC.

Temperature showed an influence on the adsorption of BAC, especially for the dyes MB and BCG. The distribution coefficient (Kd), which indicates the affinity of the adsorbate for the adsorbent [21], presented higher values at higher temperatures, suggesting an increasing affinity in these cases. MB exhibited the highest q_{max} values, highlighting a greater affinity for the active sites of all three carbons. On the other hand, BCG showed an increase in adsorption with rising temperature, but maintained low Kd values, indicating relatively lower affinity compared to MB. The adsorption of MR showed a distinct behavior, with q_{max} values decreasing at higher temperatures, which could be attributed to its molecular structure.

In general, temperature directly influences the adsorption efficiency of dyes onto CAC, BAC, and MAC. The thermodynamic parameters analyzed point in most cases to a spontaneous and endothermic process, with a predominant trend of higher adsorption capacity at higher temperatures. These observations are crucial for optimizing contaminated water treatment processes, contributing to the development of more sustainable solutions.

The spontaneity of the processes was determined by the variation of Gibbs free energy (ΔG). Exergonic processes ($\Delta G < 0$) are spontaneous, while endergonic processes ($\Delta G > 0$) require an input of energy [35,56,62,96]. The negative values of ΔG in most cases (Table 8) indicate that adsorption in many coal–dye combinations was spontaneous, although some combinations, such as BAC and MAC for certain dyes, presented positive ΔG values, indicating non-spontaneous adsorption under those conditions. The magnitude of ΔG generally decreases as temperature increases, reinforcing the idea that adsorption is favored at higher temperatures. For example, for MB on CAC charcoal, ΔG varied from -31.29 $kJ \cdot mol^{-1}$ to -35.12 $kJ \cdot mol^{-1}$ as the temperature increased, reflecting an improvement in the adsorption efficiency [97].

Table 8. Adsorption thermodynamics parameters of MB, BCG, and MR for CAC, BAC, and MAC (Dyes = 100 mg·L^{-1}; Activated carbons = 0.1 g; pH = 7; Volume = 50 mL).

Dye	Material	T (K)	Kd	ΔG (kJ·mol^{-1})	ΔS (J·mol^{-1}·K)	ΔH (kJ·mol^{-1})	q_{max} (mg·g^{-1})
MB	CAC	298.15	30.2918	−31.29	190.63	25.69	49.698
		308.15	35.6376	−32.75			49.746
		318.15	58.3345	−35.12			49.843
	BAC	298.15	0.6746	0.98	18.04	6.32	33.615
		308.15	0.7651	0.69			33.634
		318.15	0.7911	0.62			33.892
	MAC	298.15	3,334,519.98	−37.23	112.29	−1.91	50.000
		308.15	333,484.74	−32.58			50.000
		318.15	3,339,066.59	−39.73			50.000
BCG	CAC	298.15	29.73	−8.41	−196.19	−65.81	15.315
		308.15	3.26	−3.03			49.295
		318.15	5.77	−4.64			49.814
	BAC	298.15	0.6745	0.98	1405,09	416.50	3.407
		308.15	1.4244	−24.50			48.562
		318.15	2.3631	−26.64			49.071
	MAC	298.15	0.00279	14.58	635.88	202.07	20.630
		308.15	0.530	1.63			49.202
		318.15	0.443	2.15			49.751
MR	CAC	298.15	0.097	5.78	−113.99	−27.98	50.000
		308.15	0.051	7.62			49.801
		318.15	0.048	8.03			49.801
	BAC	298.15	0.186	4.17	−362.28	−102.95	47.451
		308.15	0.016	10.59			45.827
		318.15	0.014	11.29			46.340
	MAC	298.15	1.00	0.00	−541.23	−159.94	50.000
		308.15	0.021	9.90			49.801
		318.15	0.018	10.63			49.801

The ΔH values were mostly positive, indicating endothermic adsorption. However, some cases, such as BCG on CAC and MR on BAC and MAC, showed negative ΔH values, suggesting an exothermic nature. This corresponds to the observed trend in adsorption capacity, where adsorption increases with temperature for most cases but was more favorable at lower temperatures for others. For example, MR on CAC presented negative ΔH (−27.98 kJ·mol^{-1}) indicating that adsorption is more efficient at lower temperatures still occurs under cooler conditions [21]. The ΔS values are generally negative or very low, suggesting that adsorption reduces the disorder of the system, which can be interpreted as the organization of adsorbate molecules on the adsorbent surface. However, certain cases exhibit highly positive ΔS values, such as BAC and MAC for BCG and MR, indicating an increase in system randomness. This could be attributed to desorption phenomena or changes in the interaction mechanisms at higher temperatures [20,21].

In all cases analyzed (MB, BCG, and MR), the predominace of positive ΔH parameters and negative ΔS values suggest that the adsorption is more related to chemisorption. However, the cases with negative ΔH or positive ΔS values indicate that different mechanisms, including physisorption and structural rearrangements, may also play a role in the adsorption process [69]. MAC stood out for its structural and surface characteristics, as well

as its efficiency in removing all three dyes. Its adsorption capacity and thermodynamic parameters were compared with other precursor materials (Table 9).

Table 9. Thermodynamics parameters and maximum adsorption capacity of selected adsorbents.

Activated Carbon	ΔG ($kJ \cdot mol^{-1}$)	ΔS ($J \cdot mol^{-1} \cdot K$)	ΔH ($kJ \cdot mol^{-1}$)	q_{max} ($mg \cdot g^{-1}$)	Reference
Monguba shell	−37.23	112.29	−1.91	50.00	This work
Corn stalks	−4.59	40.11	9.53	41.00	[20]
Moringa seeds	−2.044	0.064	17.03	189.55	[69]
Copperpod leaves	−26.160	143.64	17.59	170.10	[97]
Sawdust	−8.05	0.69	193.43	75.81	[64]
Durian shell	−6.450	31.36	2.76	54.32	[36]
Macadamia nutshell	1038	−104.38	−30.40	578.93	[98]

The ΔG value for MAC was -37.23 $kJ \cdot mol^{-1}$, indicating a spontaneous and thermodynamically favorable process. Compared to other materials, such as corn stalks (-4.59 $kJ \cdot mol^{-1}$) [20] and moringa seeds (-2.044 $kJ \cdot mol^{-1}$) [69], MAC showed higher adsorption efficiency, suggesting that the process is much more favorable, providing more favorable conditions for interaction with the dyes.

Finally, although the q_{max} of MAC (50 $mg \cdot g^{-1}$) is lower than that of other materials such as moringa seeds (189.55 $mg \cdot g^{-1}$) [69] and copperpod leaves (170.10 $mg \cdot g^{-1}$) [97], its balance between efficiency and sustainability makes it a viable option, especially due to its greater accessibility and ecological advantages. This analysis emphasizes the importance of considering both the adsorption capacity and thermodynamic efficiency when evaluating materials for contaminant removal.

4. Conclusions

The chemical activation of cocoa, baru, and monguba shells with H_3PO_4 resulted in carbons possessing a pure carbon structure, enriched with functional groups that enhance adsorption performance. These materials exhibited a well-developed surface area, with MAC standing out at 1604 $m^2 \cdot g^{-1}$, achieved under impregnation conditions for 1 h, activation at 80 °C, and carbonization at 500 °C for 1 h. The performance of these carbons was promising in the adsorption of three organic dyes: MB, BCG, and MR. The adsorption kinetics of CAC, BAC, and MAC were better fitted to the pseudo-second-order model for all the dyes evaluated. In terms of equilibrium adsorption, the best performance was observed for MB, with a capacity of 50 $mg \cdot g^{-1}$, surpassing those of BCG and MR. Furthermore, the thermodynamic analysis indicated that chemisorption was the predominant process. It should be noted that all adsorption tests accounted for the progression of adsorption over time and variations in temperature.

The valorization of agricultural waste, such as cocoa, baru, and monguba shells, to produce adsorbents for the remediation of wastewater and water contaminated by dye compounds that are difficult to remove, represents a sustainable solution. This approach provides an alternative to conventional activated carbons, which are costly, and aligns with the principles of the circular economy.

5. Recommendations

Future studies should evaluate the performance of these carbon-based adsorbents at different initial concentrations of the dyes and in the presence of other components commonly found in natural waters, including an analysis under real conditions for greater representativeness. Conducting tests with shorter contact times for the target pollutant would also help optimize the project design. Additionally, it would be important to conduct

a complete lifecycle assessment (LCA), including production costs, performance, scalability, and environmental impact, as well as identify the limitations and potentialities of the proposed approach. Furthermore, fixed-bed adsorption tests could be analyzed in the future to assess the efficiency of the proposed adsorbents in real practical applications.

Supplementary Materials: The following supporting information can be downloaded at: https://www.mdpi.com/article/10.3390/su17052036/s1, Figure S1: Methylene blue (MB) calibration curve. Figure S2: Bromocresol green (BCG) calibration curve. Figure S3: Methyl red (MR) calibration curve. Figure S4: Example of calibration curve results for methylene blue. (A) Standard concentrations of methylene blue used for the calibration curve; (B) Spectrophotometer and the wavelength used (665 nm); (C) Adsorption process using monguba activated carbon showing color reduction in samples after 0, 30, and 60 min, with corresponding concentrations (100 mg·L^{-1}, 20 mg·L^{-1}, 0.1 mg·L^{-1}). Figure S5: Adsorption capacity Commercial carbon from company Dinâmica Química Contemporanea LTDA.

Author Contributions: Conceptualization, B.A.-T. and P.S.S.; methodology, B.A.-T. and M.N.E.; validation, P.S.S. and A.A.; formal analysis, B.A.-T. and G.A.-R.; investigation, B.A.-T. and M.N.E.; resources, P.S.S. and A.A.; data curation, G.A.-R.; writing—original draft preparation, B.A.-T.; writing—review and editing, P.S.S., A.A. and T.F.d.O.; visualization, P.S.S.; supervision, P.S.S.; project administration, T.F.d.O.; funding acquisition, T.F.d.O., P.S.S. and A.A. All authors have read and agreed to the published version of the manuscript.

Funding: This research was funded by CAPES—Projeto de Solidariedade Acadêmica (88881.923053/2023-01). The work was also supported by the GeoBioTec Research Unit, through the strategic projects UIDB/04035/2020 (https://doi.org/10.54499/UIDB/04035/2020) and UIDP/04035/2020 (https://doi.org/10.54499/UIDP/04035/2020), funded by the Fundação para a Ciência e a Tecnologia (FCT), IP/MCTES through national funds (PIDDAC).

Data Availability Statement: The original contributions presented in the study are included in the article, further inquiries can be directed to the corresponding author.

Acknowledgments: We are immensely grateful to Gustavo Henrique Rocha, Ana Carolina de Jesus Oliveira, Bruna Melo Miranda and Débora Murowaniecki Otero for kindly donating the cocoa, baru, and monguba residues used in this study. We also thank Macksuel Fernandes da Silva for his support in processing the residues and Paixan Febrialy Samba for her generous assistance with the Analysis of Surface Area and Porosity (ASAP).

Conflicts of Interest: The authors declare no conflicts of interest.

References

1. Bouzid, T.; Grich, A.; Naboulsi, A.; Regti, A.; Alaoui Tahiri, A.; El Himri, M.; El Haddad, M. Adsorption of Methyl Red on Porous Activated Carbon from Agriculture Waste: Characterization and Response Surface Methodology Optimization. *Inorg. Chem. Commun.* **2023**, *158*, 111544. [CrossRef]
2. Ani, J.U.; Akpomie, K.G.; Okoro, U.C.; Aneke, L.E.; Onukwuli, O.D.; Ujam, O.T. Potentials of Activated Carbon Produced from Biomass Materials for Sequestration of Dyes, Heavy Metals, and Crude Oil Components from Aqueous Environment. *Appl. Water Sci.* **2020**, *10*, 69. [CrossRef]
3. Aichour, A.; Zaghouane-Boudiaf, H.; Khodja, H.D. Highly Removal of Anionic Dye from Aqueous Medium Using a Promising Biochar Derived from Date Palm Petioles: Characterization, Adsorption Properties and Reuse Studies. *Arab. J. Chem.* **2022**, *15*, 103542. [CrossRef]
4. Sponza, D.T.; Işık, M. Decolorization and Inhibition Kinetic of Direct Black 38 Azo Dye with Granulated Anaerobic Sludge. *Enzym. Microb. Technol.* **2004**, *34*, 147–158. [CrossRef]
5. Tony, B.D.; Goyal, D.; Khanna, S. Decolorization of Textile Azo Dyes by Aerobic Bacterial Consortium. *Int. Biodeterior. Biodegrad.* **2009**, *63*, 462–469. [CrossRef]
6. Xu, H.; Zheng, H.-Y.; Liu, C.-H. Methyl Red Degradation by a Subseafloor Fungus Schizophyllum Commune 15R-5-F01: Efficiency, Pathway, and Product Toxicity. *3 Biotech* **2024**, *14*, 202. [CrossRef]

7. Xue, H.; Wang, X.; Xu, Q.; Dhaouadi, F.; Sellaoui, L.; Seliem, M.K.; Ben Lamine, A.; Belmabrouk, H.; Bajahzar, A.; Bonilla-Petriciolet, A.; et al. Adsorption of Methylene Blue from Aqueous Solution on Activated Carbons and Composite Prepared from an Agricultural Waste Biomass: A Comparative Study by Experimental and Advanced Modeling Analysis. *Chem. Eng. J.* **2022**, *430*, 132801. [CrossRef]
8. Patel, P.; Gupta, S.; Mondal, P. Modeling and Optimization of Process Parameters of MB Dye Adsorption Using Waste-Derived Chemically Activated Biosorbents. *Biomass Convers. Biorefinery* **2023**, *13*, 13461–13480. [CrossRef]
9. Elkholy, A.S.; Yahia, M.S.; Elnwawy, M.A.; Gomaa, H.A.; Elzaref, A.S. Synthesis of Activated Carbon Composited with Egyptian Black Sand for Enhanced Adsorption Performance toward Methylene Blue Dye. *Sci. Rep.* **2023**, *13*, 4209. [CrossRef]
10. Egbosiuba, T.C.; Abdulkareem, A.S.; Kovo, A.S.; Afolabi, E.A.; Tijani, J.O.; Auta, M.; Roos, W.D. Ultrasonic Enhanced Adsorption of Methylene Blue onto the Optimized Surface Area of Activated Carbon: Adsorption Isotherm, Kinetics and Thermodynamics. *Chem. Eng. Res. Des.* **2020**, *153*, 315–336. [CrossRef]
11. Tran, T.H.; Le, H.H.; Pham, T.H.; Nguyen, D.T.; La, D.D.; Chang, S.W.; Lee, S.M.; Chung, W.J.; Nguyen, D.D. Comparative Study on Methylene Blue Adsorption Behavior of Coffee Husk-Derived Activated Carbon Materials Prepared Using Hydrothermal and Soaking Methods. *J. Environ. Chem. Eng.* **2021**, *9*, 105362. [CrossRef]
12. National Center for Biotechnology Information. Methylene Blue, PubChem Compound Summary for CID 6099. Available online: https://pubchem.ncbi.nlm.nih.gov/compound/Methylene-blue (accessed on 15 August 2024).
13. Onu, C.E.; Ohale, P.E.; Ekwueme, B.N.; Obiora-Okafo, I.A.; Okey-Onyesolu, C.F.; Onu, C.P.; Ezema, C.A.; Onu, O.O. Modeling, Optimization, and Adsorptive Studies of Bromocresol Green Dye Removal Using Acid Functionalized Corn Cob. *Clean. Chem. Eng.* **2022**, *4*, 100067. [CrossRef]
14. Suditu, G.D.; Drăgoi, E.N.; Apostică, A.G.; Mănăilă, A.M.; Radu, V.M.; Puițel, A.C.; Nechita, M.T. Artificial Intelligence-Based Tools for Process Optimization: Case Study—Bromocresol Green Decolorization with Active Carbon. *Adsorpt. Sci. Technol.* **2022**, *2022*, 8110436. [CrossRef]
15. Liu, D.; Yuan, J.; Li, J.; Zhang, G. Preparation of Chitosan Poly(Methacrylate) Composites for Adsorption of Bromocresol Green. *ACS Omega* **2019**, *4*, 12680–12686. [CrossRef]
16. Awokoya, K.N.; Oninla, V.O.; Ogunkunle, O.A.; Oyebode, B.A.; Owoade, O.J.; Obitusin, O.O.; Ipadeola, D.T. Preparation of Styrene-Based Imprinted Polymer for the Adsorption of Hazardous Bromocresol Green Dye: Equilibrium, Kinetics and Thermodynamics Study. *Ife J. Sci.* **2024**, *26*, 45–57. [CrossRef]
17. National Center for Biotechnology Information. Bromocresol Green, PubChem Compound Summary for CID 6451. Available online: https://pubchem.ncbi.nlm.nih.gov/compound/Bromocresol-green (accessed on 15 August 2024).
18. Romdhane, D.F.; Satlaoui, Y.; Nasraoui, R.; Charef, A.; Azouzi, R. Adsorption, Modeling, Thermodynamic, and Kinetic Studies of Methyl Red Removal from Textile-Polluted Water Using Natural and Purified Organic Matter Rich Clays as Low-Cost Adsorbent. *J. Chem.* **2020**, *2020*, 4376173. [CrossRef]
19. Ghazoui, M.; Elkacmi, R.; Sylla, A.S.; Moulakhnif, K.; Touzani, I.; Boudouch, O. Efficient Removal of Methylene Blue and Methyl Red Dyes Using a Novel Adsorbent Derived from *Saponaria Officinalis* Root via H_3PO_4, H_2SO_4, and KOH-Activation: Optimization, Kinetics, and Isotherm Study. *Desalination Water Treat.* **2024**, *318*, 100378. [CrossRef]
20. Wolski, R.; Bazan-Wozniak, A.; Pietrzak, R. Adsorption of Methyl Red and Methylene Blue on Carbon Bioadsorbents Obtained from Biogas Plant Waste Materials. *Molecules* **2023**, *28*, 6712. [CrossRef]
21. Lafi, R.; Abdellaoui, L.; Montasser, I.; Mabrouk, W.; Hafiane, A. The Effect of Head Group of Surfactant on the Adsorption of Methyl Red onto Modified Coffee Residues. *J. Mol. Struct.* **2022**, *1249*, 131527. [CrossRef]
22. National Center for Biotechnology Information. Methyl Red, PubChem Compound Summary for CID 10303. Available online: https://pubchem.ncbi.nlm.nih.gov/compound/Methyl-red (accessed on 15 August 2024).
23. Aguiar, T.; Baumann, L.; Albuquerque, A.; Teixeira, L.; Gil, E.; Scalize, P. Application of Electrocoagulation for the Removal of Transition Metals in Water. *Sustainability* **2023**, *15*, 1492. [CrossRef]
24. Omo-Okoro, P.N.; Daso, A.P.; Okonkwo, J.O. A Review of the Application of Agricultural Wastes as Precursor Materials for the Adsorption of Per- and Polyfluoroalkyl Substances: A Focus on Current Approaches and Methodologies. *Environ. Technol. Innov.* **2018**, *9*, 100–114. [CrossRef]
25. Sadh, P.K.; Duhan, S.; Duhan, J.S. Agro-Industrial Wastes and Their Utilization Using Solid State Fermentation: A Review. *Bioresour. Bioprocess.* **2018**, *5*, 1. [CrossRef]
26. Melo, B.; Alvez, B.; Otero, D.; Da Silva, F.; Scalize, P.; De Oliveira, T. By-Products of Baru and Monguba: A Review of Their Potential. *Food Humanit.* **2024**, *4*, 100477. [CrossRef]
27. Tapia, Y.M.; de Oliveira, T.F.; Gabriel, E.F.M.; Scalize, P.S. Use of Agroindustrial Materials as Activated Carbon Precursors for Caffeine Removal: Global Overview. *Rev. Gest. Soc. E Ambient.* **2023**, *17*, e03430. [CrossRef]
28. Alves, A.C.F.; Barbosa, J.G.; De Oliveira, S.B.; Scalize, P.S. Polymeric Hydrochars Produced from Ion Exchange Resin Residue Applied in the Removal of Emerging Contaminants in Water. *Int. J. Environ. Sci. Technol.* **2025**, *22*, 79–98. [CrossRef]

29. Gonçalves, J.O.; De Farias, B.S.; Rios, E.C.; Ribeiro, A.C.; Acosta, K.D.R.; Gomes, C.P.W.; Cadaval Junior, T.R. Sustainable Removal of Chloroquine from Aqueous Solutions Using Microwave-Activated Cassava Biochar Derived from Agricultural Waste. *Sustainability* **2024**, *16*, 9854. [CrossRef]
30. Henao-Toro, H.; Pérez, J.F.; Rubio-Clemente, A. Malachite Green Dye Removal in Water by Using Biochar Produced from Pinus Patula Pellet Gasification in a Reverse Downdraft Reactor. *Sustainability* **2024**, *16*, 11043. [CrossRef]
31. Chen, S.C.; Dang, X.; Xu, Q.; Own, C.-M. Transforming Waste into Value: Sustainable Recycling of Agricultural Resources Under the 'Carbon Peak and Carbon Neutrality' Vision. *Sustainability* **2024**, *17*, 55. [CrossRef]
32. Cano, F.J.; Reyes-Vallejo, O.; Sánchez-Albores, R.M.; Sebastian, P.J.; Cruz-Salomón, A.; Hernández-Cruz, M.D.C.; Montejo-López, W.; González Reyes, M.; Serrano Ramirez, R.D.P.; Torres-Ventura, H.H. Activated Biochar from Pineapple Crown Biomass: A High-Efficiency Adsorbent for Organic Dye Removal. *Sustainability* **2024**, *17*, 99. [CrossRef]
33. Alves, A.C.F.; Antero, R.V.P.; De Oliveira, S.B.; Ojala, S.A.; Scalize, P.S. Activated Carbon Produced from Waste Coffee Grounds for an Effective Removal of Bisphenol-A in Aqueous Medium. *Environ. Sci. Pollut. Res.* **2019**, *26*, 24850–24862. [CrossRef]
34. Zuhara, S.; McKay, G. Waste-Derived Activated Carbons for Effective Adsorptive Removal of Strontium, Barium, and Binary Pollutants: A Response Surface Methodology Study. *J. Environ. Chem. Eng.* **2024**, *12*, 112836. [CrossRef]
35. Metyouy, K.; Benkirane, L.; Sánchez, M.E.; Cara-Jiménez, J.; Plakas, K.V.; Chafik, T. Valorization of Agricultural Olive Waste as an Activated Carbon Adsorbent for the Remediation of Water Sources Contaminated with Pharmaceuticals. *Sustain. Chem. Environ.* **2024**, *6*, 100110. [CrossRef]
36. Nguyen, N.T.H.; Tran, G.T.; Nguyen, T.T.T.; Nguyen, D.T.C.; Tran, T.V. Synthesis of $MnFe_2O_4$/Activated Carbon Derived from Durian Shell Waste for Removal of Indole in Water: Optimization, Modelling, and Mechanism. *Environ. Res.* **2024**, *254*, 118883. [CrossRef] [PubMed]
37. Umoren, S.A.; Solomon, M.M.; Obot, I.B.; Suleiman, R.K. A Critical Review on the Recent Studies on Plant Biomaterials as Corrosion Inhibitors for Industrial Metals. *J. Ind. Eng. Chem.* **2019**, *76*, 91–115. [CrossRef]
38. Mahesh, N.; Balakumar, S.; Shyamalagowri, S.; Manjunathan, J.; Pavithra, M.K.S.; Babu, P.S.; Kamaraj, M.; Govarthanan, M. Carbon-Based Adsorbents as Proficient Tools for the Removal of Heavy Metals from Aqueous Solution: A State of Art-Review Emphasizing Recent Progress and Prospects. *Environ. Res.* **2022**, *213*, 113723. [CrossRef]
39. Pua, F.L.; Sajab, M.S.; Chia, C.H.; Zakaria, S.; Rahman, I.A.; Salit, M.S. Alkaline-Treated Cocoa Pod Husk as Adsorbent for Removing Methylene Blue from Aqueous Solutions. *J. Environ. Chem. Eng.* **2013**, *1*, 460–465. [CrossRef]
40. Santana, A.J.; Dos Santos, W.N.L.; Silva, L.O.B.; Das Virgens, C.F. Removal of Mercury(II) Ions in Aqueous Solution Using the Peel Biomass of *Pachira Aquatica* Aubl: Kinetics and Adsorption Equilibrium Studies. *Environ. Monit. Assess.* **2016**, *188*, 293. [CrossRef]
41. Nascimento, T.L.S.; Oliveira, K.F.S.; Junior, J.O.D.; Pimenta, A.S.; Melo, D.M.A.; Melo, M.A.F.; Braga, R.M. Biosorption of Nickel and Cadmium Using *Pachira Aquatica* Aubl. Peel Biochar. *Sci. Rep.* **2024**, *14*, 5086. [CrossRef]
42. Oliveira, T.F.; Oliveira, A.C.J.; Marsico, E.T.; Valdés, H. Development of a Porous Material Based on Baru (*Dipteryx alata* Vog.) and Its Effect on the Post-Harvest Storage of Bananas. *Investig. Joven* **2024**, *10*, 124.
43. Ramutshatsha-Makhwedzha, D.; Mavhungu, A.; Moropeng, M.L.; Mbaya, R. Activated Carbon Derived from Waste Orange and Lemon Peels for the Adsorption of Methyl Orange and Methylene Blue Dyes from Wastewater. *Heliyon* **2022**, *8*, e09930. [CrossRef]
44. Tandazo, T.C.; Romero, M.E.Y.; Balarezo, C.B.; Reyes, E.E.; Loaiza, A.V. Carbón Activado a Partir de Residuos de Cáñamo Modificado Químicamente Para Remover Azul de Metileno. *Cienc. Lat. Rev. Científica Multidiscip.* **2023**, *7*, 2536–2552. [CrossRef]
45. Li, X.; Jia, H.; Jiang, L.; Mou, Z.; Zhang, B.; Zhang, Z.; Chen, Y. Biochar Prepared from Steam-Exploded Bitter Melon Vine for the Adsorption of Methylene Blue from Aqueous Solution: Kinetics, Isotherm, Thermodynamics and Mechanism. *Sustainability* **2024**, *16*, 7278. [CrossRef]
46. Vásquez, Z.S.; Neto, D.P.D.C.; Pereira, G.V.M.; Vandenberghe, L.P.S.; De Oliveira, P.Z.; Tiburcio, P.B.; Rogez, H.L.G.; Neto, A.G.; Soccol, C.R. Biotechnological Approaches for Cocoa Waste Management: A Review. *Waste Manag.* **2019**, *90*, 72–83. [CrossRef] [PubMed]
47. Sano, S.M.; De Brito, M.A.; Ribeiro, J.F. Dipteryx Alata (Baru). In *Espécies Nativas da Flora Brasileira de Valor Econômico Atual ou Potencial: Plantas Para o Futuro—Região Centro-Oeste*; Vieira, R.F., Camilo, J., Coradin, L., Brazil, Eds.; Biodiversidade; MMA, Ministério do Meio Ambiente: Brasília, Brazil, 2016; Volume 44, pp. 203–215, ISBN 978-85-7738-309-2.
48. Lima, D.C.; Alves, M.D.R.; Noguera, N.H.; Nascimento, R.D.P.D. A Review on Brazilian Baru Plant (*Dipteryx alata* Vogel): Morphology, Chemical Composition, Health Effects, and Technological Potential. *Future Foods* **2022**, *5*, 100146. [CrossRef]
49. Rodrigues, A.P.; Náthia-Neves, G.; Pereira, G.A.; Massarioli, A.P.; Meireles, M.Â.D.A.; De Alencar, S.M.; Pastore, G.M. Obtaining High-Quality Oil from Monguba (*Pachira Aquatica* Aubl.) Seeds by Using Supercritical CO_2 Process. *J. Supercrit. Fluids* **2021**, *171*, 105192. [CrossRef]
50. Singh, M.; Agarwal, S.; Agarwal, M. Rachana benefits of *Theobroma cacao* and its phytocompounds as cosmeceuticals. In *Plant-Derived Bioactives*; Swamy, M.K., Ed.; Springer: Singapore, 2020; pp. 509–521, ISBN 978-981-15-1760-0.

51. Chañi-Paucar, L.O.; Osorio-Tobón, J.F.; Johner, J.C.F.; Meireles, M.A.A. A Comparative and Economic Study of the Extraction of Oil from Baru (*Dipteryx Alata*) Seeds by Supercritical CO_2 with and without Mechanical Pressing. *Heliyon* **2021**, *7*, e05971. [CrossRef]
52. Azizah, A.N.; Yuniastuti, E.; Nandariyah; Supriyono; Putri, I.I.S. Morphological Characterization of Pachira (*Pachira aquatica* Aubl.). *IOP Conf. Ser. Earth Environ. Sci.* **2021**, *905*, 012044. [CrossRef]
53. *ChemSketch (Freeware)*, Version 2023.2.4: ACD/Labs; Advanced Chemistry Development, Inc.: Toronto, ON, Canada, 2023. Available online: http://www.acdlabs.com (accessed on 4 February 2024).
54. Boundzanga, H.M.; Cagnon, B.; Roulet, M.; De Persis, S.; Vautrin-Ul, C.; Bonnamy, S. Contributions of Hemicellulose, Cellulose, and Lignin to the Mass and the Porous Characteristics of Activated Carbons Produced from Biomass Residues by Phosphoric Acid Activation. *Biomass Convers. Biorefinery* **2022**, *12*, 3081–3096. [CrossRef]
55. Pereira, R.G.; Veloso, C.M.; Da Silva, N.M.; De Sousa, L.F.; Bonomo, R.C.F.; De Souza, A.O.; Souza, M.O.D.G.; Fontan, R.D.C.I. Preparation of Activated Carbons from Cocoa Shells and Siriguela Seeds Using H_3PO_4 and $ZnCL_2$ as Activating Agents for BSA and α-Lactalbumin Adsorption. *Fuel Process. Technol.* **2014**, *126*, 476–486. [CrossRef]
56. Nascimento, R.F.D.; Lima, A.C.A.D.; Vidal, C.B.; Melo, D.D.Q.; Raulino, G.S.C. *Adsorção: Aspectos Teóricos e Aplicações Ambientais*; Estudos da Pós- Graduação; Imprensa Universitária—Universidade Federal do Ceará: Fortaleza, Brazil, 2020; ISBN 978-65-990722-7-7.
57. Park, J.; Regalbuto, J.R. A Simple, Accurate Determination of Oxide PZC and the Strong Buffering Effect of Oxide Surfaces at Incipient Wetness. *J. Colloid Interface Sci.* **1995**, *175*, 239–252. [CrossRef]
58. Bakatula, E.N.; Richard, D.; Neculita, C.M.; Zagury, G.J. Determination of Point of Zero Charge of Natural Organic Materials. *Environ. Sci. Pollut. Res.* **2018**, *25*, 7823–7833. [CrossRef] [PubMed]
59. Rouquerol, J.; Llewellyn, P.; Rouquerol, F. Is the Bet Equation Applicable to Microporous Adsorbents? In *Studies in Surface Science and Catalysis*; Elsevier: Amsterdam, The Netherlands, 2007; Volume 160, pp. 49–56, ISBN 978-0-444-52022-7.
60. Jagiello, J. Stable Numerical Solution of the Adsorption Integral Equation Using Splines. *Langmuir* **1994**, *10*, 2778–2785. [CrossRef]
61. Gupta, S.S.; Bhattacharyya, K.G. Kinetics of Adsorption of Metal Ions on Inorganic Materials: A Review. *Adv. Colloid Interface Sci.* **2011**, *162*, 39–58. [CrossRef] [PubMed]
62. Nascimento, J.S.; Camelo, E.R.; Carvalho, M.S.; Virgens, C.F. Kinetic Evaluation of *Pachira Aquatica* Aubl Biomass Slow Pyrolysis towards to Biochar Production. *Biofuels* **2024**, *15*, 615–625. [CrossRef]
63. Khan, T.A.; Nouman, M.; Dua, D.; Khan, S.A.; Alharthi, S.S. Adsorptive Scavenging of Cationic Dyes from Aquatic Phase by H_3PO_4 Activated Indian Jujube (*Ziziphus mauritiana*) Seeds Based Activated Carbon: Isotherm, Kinetics, and Thermodynamic Study. *J. Saudi Chem. Soc.* **2022**, *26*, 101417. [CrossRef]
64. Amellal, T.; Boukhalfa, N.; Meniai, A.H. Enhanced Removal of Basic Brown1 Dye from Aqueous Solutions by Sawdust Activated Carbon. Equilibrium, Thermodynamic and Kinetics. *Desalination Water Treat.* **2024**, *317*, 100057. [CrossRef]
65. Prahas, D.; Kartika, Y.; Indraswati, N.; Ismadji, S. Activated Carbon from Jackfruit Peel Waste by H_3PO_4 Chemical Activation: Pore Structure and Surface Chemistry Characterization. *Chem. Eng. J.* **2008**, *140*, 32–42. [CrossRef]
66. Piccoli, V.; Gonçalves, G.D.R.; Cipriano, D.F.; Freitas, J.C.C.; Schettino, M.A., Jr. Production of Phosphorus-Containing Activated Carbons from Coffee Husk and Application in Adsorption Processes. *Rev. Virtual Quím.* **2020**, *12*, 75–88. [CrossRef]
67. Queiroz, L.S.; De Souza, L.K.C.; Thomaz, K.T.C.; Lima, E.T.L.; Da Rocha Filho, G.N.; Do Nascimento, L.A.S.; Pires, L.H.D.O.; Faial, K.D.C.F.; Da Costa, C.E.F. Activated Carbon Obtained from Amazonian Biomass Tailings (Acai Seed): Modification, Characterization, and Use for Removal of Metal Ions from Water. *J. Environ. Manag.* **2020**, *270*, 110868. [CrossRef]
68. Phothong, K.; Tangsathitkulchai, C.; Lawtae, P. The Analysis of Pore Development and Formation of Surface Functional Groups in Bamboo-Based Activated Carbon during CO_2 Activation. *Molecules* **2021**, *26*, 5641. [CrossRef]
69. Raji, Y.; Nadi, A.; Mechnou, I.; Saadouni, M.; Cherkaoui, O.; Zyade, S. High Adsorption Capacities of Crystal Violet Dye by Low-Cost Activated Carbon Prepared from Moroccan *Moringa oleifera* Wastes: Characterization, Adsorption and Mechanism Study. *Diam. Relat. Mater.* **2023**, *135*, 109834. [CrossRef]
70. Pezoti, O.; Cazetta, A.L.; Bedin, K.C.; Souza, L.S.; Martins, A.C.; Silva, T.L.; Santos Júnior, O.O.; Visentainer, J.V.; Almeida, V.C. NaOH-Activated Carbon of High Surface Area Produced from Guava Seeds as a High-Efficiency Adsorbent for Amoxicillin Removal: Kinetic, Isotherm and Thermodynamic Studies. *Chem. Eng. J.* **2016**, *288*, 778–788. [CrossRef]
71. Harabi, S.; Guiza, S.; Álvarez-Montero, A.; Gómez-Avilés, A.; Bagané, M.; Belver, C.; Bedia, J. Adsorption of Pesticides on Activated Carbons from Peach Stones. *Processes* **2024**, *12*, 238. [CrossRef]
72. Wang, H.; Li, Z.; Yahyaoui, S.; Hanafy, H.; Seliem, M.K.; Bonilla-Petriciolet, A.; Luiz Dotto, G.; Sellaoui, L.; Li, Q. Effective Adsorption of Dyes on an Activated Carbon Prepared from Carboxymethyl Cellulose: Experiments, Characterization and Advanced Modelling. *Chem. Eng. J.* **2021**, *417*, 128116. [CrossRef]
73. Zięzio, M.; Charmas, B.; Jedynak, K.; Hawryluk, M.; Kucio, K. Preparation and Characterization of Activated Carbons Obtained from the Waste Materials Impregnated with Phosphoric Acid(V). *Appl. Nanosci.* **2020**, *10*, 4703–4716. [CrossRef]

74. Mekuiko, A.Z.; Tchuifon, D.R.T.; Kouteu, P.A.N.; Fotsop, C.G.; Ngakou, C.S.; Kuete, H.-I.T.; Bopda, A.; Tamo, A.K.; Anagho, S.G. Tailoring Activated Carbons Based Cocoa Pods Lignocellulosic Materials for Reactive Blue 19 Adsorption: Optimization, Adsorption Isotherm and Kinetic Investigation. *Desalination Water Treat.* **2023**, *300*, 144–157. [CrossRef]
75. Yang, Z.; Gleisner, R.; Mann, D.H.; Xu, J.; Jiang, J.; Zhu, J.Y. Lignin Based Activated Carbon Using H_3PO_4 Activation. *Polymers* **2020**, *12*, 2829. [CrossRef]
76. Dos Santos, H.V.R.; Scalize, P.S.; Teran, F.J.C.; Cuba, R.M.F. Fluoride Removal from Aqueous Medium Using Biochar Produced from Coffee Ground. *Resources* **2023**, *12*, 84. [CrossRef]
77. Puziy, A.M.; Poddubnaya, O.I.; Ziatdinov, A.M. On the Chemical Structure of Phosphorus Compounds in Phosphoric Acid-Activated Carbon. *Appl. Surf. Sci.* **2006**, *252*, 8036–8038. [CrossRef]
78. Mopoung, S.; Amornsakch, P. Microporous Activated Carbon Fiber from Pineapple Leaf Fiber by H_3PO_4 Activation. *Asian J. Sci. Res.* **2015**, *9*, 24–33. [CrossRef]
79. Rubangakene, N.O.; Elwardany, A.; Fujii, M.; Sekiguchi, H.; Elkady, M.; Shokry, H. Biosorption of Congo Red Dye from Aqueous Solutions Using Pristine Biochar and ZnO Biochar from Green Pea Peels. *Chem. Eng. Res. Des.* **2023**, *189*, 636–651. [CrossRef]
80. Neme, I.; Gonfa, G.; Masi, C. Activated Carbon from Biomass Precursors Using Phosphoric Acid: A Review. *Heliyon* **2022**, *8*, e11940. [CrossRef] [PubMed]
81. Sing, K.S.W.; Everett, D.H.; Haul, R.A.W.; Moscou, L.; Pierotti, R.A.; Rouquerol, J.; Siemieniewska, T. Reporting Physisorption Data for Gas/Solid Systems with Special Reference to the Determination of Surface Area and Porosity (Recommendations 1984). *Pure Appl. Chem.* **1985**, *57*, 603–619. [CrossRef]
82. Renner, T. *Quantities, Units and Symbols in Physical Chemistry*; Cohen, E.R., Cvitas, T., Frey, J.G., Holström, B., Kuchitsu, K., Marquardt, R., Mills, I., Pavese, F., Quack, M., et al., Eds.; The Royal Society of Chemistry: Cambridge, UK, 2007; ISBN 978-0-85404-433-7.
83. Rouquérol, F.; Rouquerol, J.; Sing, K.S.W.; Llewellyn, P.L.; Maurin, G. *Adsorption by Powders and Porous Solids: Principles, Methodology and Applications*, 2nd ed.; Elsevier/AP: Amsterdam, The Netherlands, 2014; ISBN 978-0-08-097035-6.
84. Thommes, M.; Kaneko, K.; Neimark, A.V.; Olivier, J.P.; Rodriguez-Reinoso, F.; Rouquerol, J.; Sing, K.S.W. Physisorption of Gases, with Special Reference to the Evaluation of Surface Area and Pore Size Distribution (IUPAC Technical Report). *Pure Appl. Chem.* **2015**, *87*, 1051–1069. [CrossRef]
85. Zienkiewicz-Strzalka, M.; Blachnio, M.; Derylo-Marczewska, A.; Winter, S.; Maciejewska, M. Mesoporous Carbons and Highly Cross-Linking Polymers for Removal of Cationic Dyes from Aqueous Solutions—Studies on Adsorption Equilibrium and Kinetics. *Materials* **2024**, *17*, 1374. [CrossRef]
86. Lagergren, S. About the Theory of So-Called Adsorption of Soluble Substances. *K. Sven. Vetenskapsakademiens Handl.* **1898**, *24*, 1–39.
87. Ho, Y.S.; McKay, G. Pseudo-Second Order Model for Sorption Processes. *Process Biochem.* **1999**, *34*, 451–465. [CrossRef]
88. Hu, W.; Zhang, X.; Chen, M.; Rahman, S.T.; Li, X.; Wang, G. Enhancing Cr (VI) Adsorption of Chestnut Shell Biochar through H_3PO_4 Activation and Nickel Doping. *Molecules* **2024**, *29*, 2220. [CrossRef]
89. Onu, C.E.; Asadu, C.O.; Ohale, P.E.; Nweke, C.N.; Nwokedi, I.C.; Musei, N.N.; Onu, C.P. Adsorptive Removal of Bromocresol Green Dye Using Activated Corn Cob. *J. Eng. Appl. Sci.* **2022**, *21*, 824–841.
90. Kaya, N.; Uzun, Z.Y. Experimental and Modeling Studies on the Removal of Bromocresol Green from Aqueous Solutions by Using Pine Cone-Derived Activated Biochar. *Biomass Convers. Biorefinery* **2024**, *14*, 30667–30691. [CrossRef]
91. Khalfaoui, A.; Bouchareb, E.M.; Derbal, K.; Boukhaloua, S.; Chahbouni, B.; Bouchareb, R. Uptake of Methyl Red Dye from Aqueous Solution Using Activated Carbons Prepared from *Moringa Oleifera* Shells. *Clean. Chem. Eng.* **2022**, *4*, 100069. [CrossRef]
92. Salih, S.J.; Kareem, A.S.A.; Anwer, S.S. Adsorption of Anionic Dyes from Textile Wastewater Utilizing Raw Corncob. *Heliyon* **2022**, *8*, e10092. [CrossRef] [PubMed]
93. Chen, J.; Wang, X.; Huang, Y.; Lv, S.; Cao, X.; Yun, J.; Cao, D. Adsorption Removal of Pollutant Dyes in Wastewater by Nitrogen-Doped Porous Carbons Derived from Natural Leaves. *Eng. Sci.* **2018**, *5*, 30–38. [CrossRef]
94. Jawad, A.H.; Sahu, U.K.; Mastuli, M.S.; ALOthman, Z.A.; Wilson, L.D. Multivariable Optimization with Desirability Function for Carbon Porosity and Methylene Blue Adsorption by Watermelon Rind Activated Carbon Prepared by Microwave Assisted H_3PO_4. *Biomass Convers. Biorefinery* **2024**, *14*, 577–591. [CrossRef]
95. Kopac, T.; Lin, S.D. A Review on the Characterization of Microwave-Induced Biowaste-Derived Activated Carbons for Dye Adsorption. *Int. J. Environ. Sci. Technol.* **2024**, *21*, 8717–8748. [CrossRef]
96. Hasan, I.M.; Assaf, F.H.; Tawfik, A.R. Facile and Green Synthesis of CuS-Activated Carbon Nanocomposite from Sargassum Siliquastrum Biomass for Fast and Efficient Removal of Eosin Yellow Dye. *Biomass Convers. Biorefinery* **2023**, *14*, 29873–29899. [CrossRef]

97. Reddy, Y.S.; Rotte, N.K.; Hussain, S.; Srikanth, V.V.S.S.; Chandra, M.R. Sustainable Mesoporous Graphitic Activated Carbon as Biosorbent for Efficient Adsorption of Acidic and Basic Dyes from Wastewater: Equilibrium, Kinetics and Thermodynamic Studies. *J. Hazard. Mater. Adv.* **2023**, *9*, 100214. [CrossRef]
98. Duque-Brito, E.; Lobato-Peralta, D.R.; Okolie, J.A.; Arias, D.M.; Okoye, P.U. Fast-Kinetics Adsorption of a Binary Solution Containing Cationic and Ionic Pollutants Using High-Surface Area Activated Carbon Derived from Macadamia Nutshell. *Energy Ecol. Environ.* **2023**, *9*, 84–99. [CrossRef]